Spring 2015

Delamination of C/PEKK I-Beam using virtual crack closure technique and cohesive zone method

Greeshma Ramakrishna
Purdue University

Graduate School Form 30
Updated 1/15/2015

PURDUE UNIVERSITY
GRADUATE SCHOOL
Thesis/Dissertation Acceptance

This is to certify that the thesis/dissertation prepared

By GREESHMA RAMAKRISHNA

Entitled

DELAMIANTION OF C/PEKK I-BEAM USING VIRTUAL CRACK CLOSURE TECHNIQUE AND COHESIVE ZONE METHOD

For the degree of Master of Science in Aeronautics and Astronautics

Is approved by the final examining committee:

VIKAS TOMAR
Chair

R. BYRON PIPES
Co-chair

WENBIN YU
Co-chair

To the best of my knowledge and as understood by the student in the Thesis/Dissertation Agreement, Publication Delay, and Certification Disclaimer (Graduate School Form 32), this thesis/dissertation adheres to the provisions of Purdue University's "Policy of Integrity in Research" and the use of copyright material.

Approved by Major Professor(s): VIKAS TOMAR

Approved by: WEINONG CHEN 4/22/2015

Head of the Departmental Graduate Program Date

DELAMINATION OF C/PEKK I-BEAM USING VIRTUAL CRACK CLOSURE TECHNIQUE AND COHESIVE ZONE METHOD

A Thesis

Submitted to the Faculty

of

Purdue University

by

Greeshma Ramakrishna

In Partial Fulfillment of the

Requirements for the Degree

of

Master of Science in Aeronautics and Astronautics

May 2015

Purdue University

West Lafayette, Indiana

Dedicated to the memory of my grandfather, Dr. L Rudrappa

ACKNOWLEDGEMENTS

I would like to extend immeasurable appreciation and deepest gratitude for the help and support of the following people who in one way or another have contributed in making this study possible.

To Dr. Vikas Tomar, for his constant support and provisions that helped me in the successful completion of my thesis. Without his faith and guidance, I could not have finished my studies on time

To all my colleagues at the Interfacial Multiphysics Lab, especially Tao Qu, for their help with my research

To Mr. Pieter Lantermans and all the employees at Fokker Aerostructures B.V, for believing in me and giving me an opportunity to work with them

To Mr. Mihir Bhagat, for his untiring support and always motivating me to work harder

To Akanksha Ramakrishna and my family for their unaltering faith and love, always reminding me of my priorities

Finally, to my parents, Mrs. Nandini R and Sqn. Ldr. K N Ramakrishna, for their sacrifices, support and constant belief in me. You are and always will be my inspiration

TABLE OF CONTENTS

Page

Page

LIST OF TABLES

Table Page

LIST OF FIGURES

Figure Page

Figure Page

ABSTRACT

Ramakrishna, Greeshma. M.S., Purdue University, May 2015. Delamination of C/PEKK I-Beam Using Virtual Crack Closure Technique and Cohesive Zone Method. Major Professor: Vikas Tomar.

In collaboration with Fokker Aerostructures B.V, a damage study is conducted on a carbon epoxy/PEKK (poly-ether-ketone-ketone) thermoplastic composite I-Beam, with a pre crack of 100 mm modeled between the top flange and the filler (butt joint between filler and web). The C/PEKK I-Beam is modeled after a section of the Gulfstream G650 aircraft's center beam, which was previously a carbon fiber/epoxy hat-stiffened skin construction. The objective of the thesis is to identify if the crack propagates in the I-Beam within the load range that act on the current center beam of the G650 aircraft. Two finite element methods are identified to study the crack propagation in the model, namely virtual crack closure technique (VCCT) and the cohesive zone model (CZM). These two methods are verified by reproducing experimental data for calculating fracture toughness (mode I and mode II) of PEKK thermoplastic produced by CYTEC Inc., using ABAQUS CAE. Next, the I-Beam is modeled under a four point bending load, and analysis is performed using both the methods to study the loads at which the model begins to delaminate. Both the approaches produce similar data, verifying the results obtained. The model does delaminate within the range of the loads applied on the center beam.

CHAPTER 1. INTRODUCTION

1.1 Background

The goal of the aerospace industry is to satisfy customer requirements by enhancing aircraft performance and minimizing acquisition and operating costs. Achieving this goal is reliant in part on the development of 'superior' structural materials. Over the past 70 years, aluminum has been the dominant aerospace structural material. Polymer matrix composites, on the other hand, were not used in large amounts until the1990s. The use of composites in aerospace applications has increased greatly in the past decade. In 1982, 8% of the airbus A130 consisted of composites. Twenty years later, the use of composites in Airbus A380 rose to 25%. In the current generation of aircrafts, Boeing flew the 787 Dreamliner in 2009, which was made of 50% composites, and in June 2013 Airbus flew its Airbus A350 XWB which is made up of 53% composites. Composites are conquering traditional metal domains throughout the aircraft. In the military sector, about 35% of the structural weight of the Airbus A-400M is composite material. As other examples, composites account for about 25% and 35% of the Lockheed Martin F-22 Raptor and F-35 Lighting II, respectively. Figure 1.1 shows the rapid increase in the composition of material in the airframe with time.

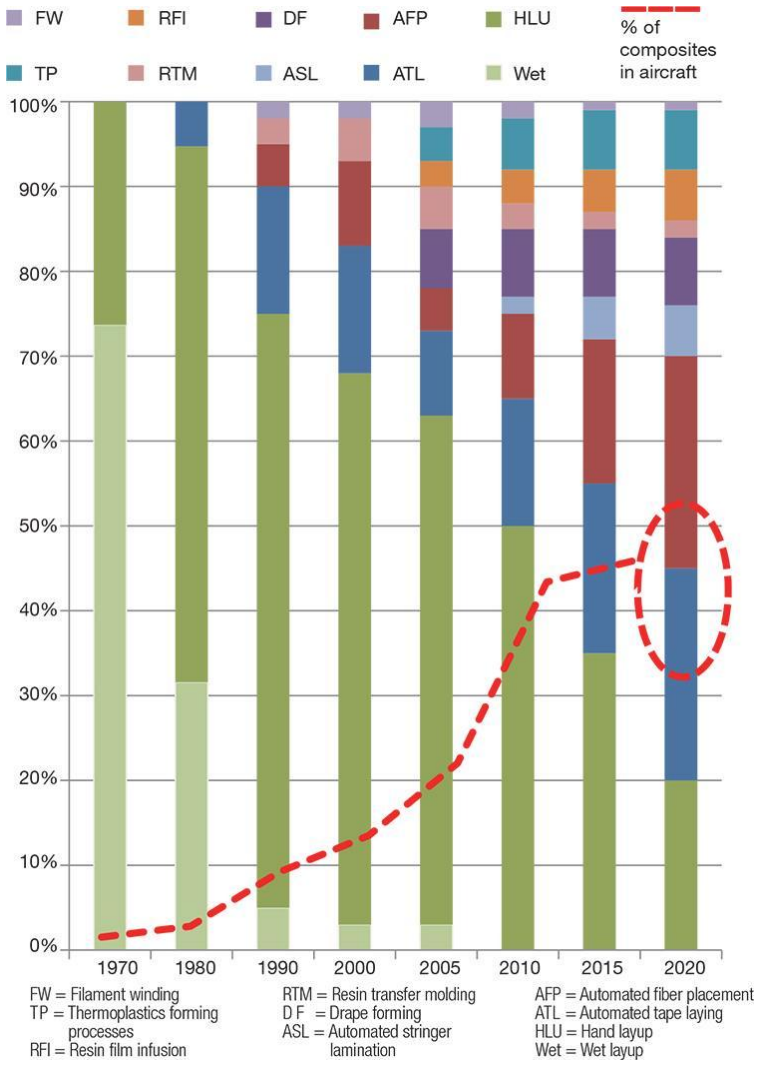

Figure 1-1 Change in Composite Manufacture Processes vs. Airframe content.

The large increase in the use of composites in aerospace applications is because they provide important benefits over aluminum alloys, including lighter weight which results in more fuel efficient and environmental friendly aircraft (less NOx and greenhouse gas emissions from fuel burn) thus increasing aircraft range, payload or maneuverability; form into more complex shapes/design; offer the capability to be stacked/designed in such a way that the properties of the composite is tailored to best withstand loads; fewer number of components, fasteners and joints; higher specific

strength, specific stiffness and fatigue resistance; excellent chemical and corrosion resistance; and good acoustic insulation and vibration damping properties.

Today, vast majority of composite materials for aerospace are based on thermoset materials, especially in the United States. Thermoset composites have a successful track record dating back to 1960s, making the database very reliable. However, the second half of the 1980s saw the emergence of a new family of composite materials, continuous fiber reinforced thermoplastics and for the past two decades, they have significantly matured. These composites have several key advantages over thermosets. Since thermoset composite processes and materials are mature, cost and weight reduction associated with design optimizations are less likely to continue. However, since the research with regards to thermoplastics is still ongoing, it is easy to mold it to the needs of the evolving aerospace requirements.

These thermoplastic composites are comparable to thermoset composites in the sense that they have the same fiber reinforcements as carbon, aramid or glass fiber fabrics or unidirectional tapes. However, a lot of justifications can be made for using higher-cost thermoplastic composites instead of thermoset composites in aerospace applications. Unlike thermosets, thermoplastics polymers shape easily under sufficient heat and simply harden and maintain those shapes when cooled. They also retain their plasticity — that is, they will remelt and can be reshaped by reheating them above their processing temperatures. This characteristic offers intriguing

possibilities for both faster and more innovative composite processing techniques compared to their thermoset counterparts.

Thus, as a result of this paradigm shift toward *process/cost efficiency*, reinforced thermoplastics now appear on the cusp of capturing a significant piece of the aerospace raw materials market as seen in Fig 1.1.

1.2 Thermoplastic Composites: What and Why

There is a wide range of thermoplastic materials now used in advanced composites components for the aerospace industry.[1] Six general classes of thermoplastics are seen most frequently

- Poly-carbonates (PC)
- Poly-amides (nylon, PA-6, PA-12)
- Poly-phenylene +Sulfide (PPS)[2]
- Poly-ether-imide (PEI)[3]
- Poly-ether-ether-ketone (PEEK)[4]
- Poly-ether-ketone-ketone (PEKK)[5]

Continuous fibre reinforced thermoplastics have a number of advantages over other materials, a few mentioned in the previous section. Among these are improved toughness, excellent fire resistance and recyclability. However, the primary reason for the use of thermoplastics is cost effective processing. [6][7] Fig 1.2 shows a graph of neat resin performance characteristics vs. raw material costs, which makes the

potential value that thermoplastics bring to the aerospace market becomes more apparent

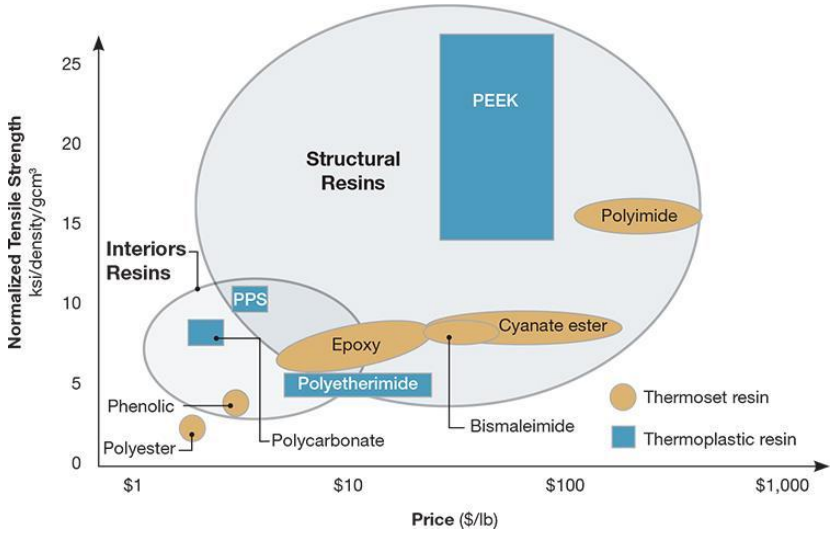

Figure 1-2 Normalized tensile Strength vs. Raw material Price for Aerospace Thermoset and Thermoplastic Polymers

Boeing and Dornier Luftfahrt have performed numerous cost-analysis studies on interior components and wind ribs respectively, confirming the cost effectiveness of thermoplastics vis-a-vis conventional materials[1][8].

PEEK, PPS, PEI and PC show many favorable characteristics for application in both aerospace structures and interior components. Although the raw material costs of aerospace thermoplastics can — in some cases — be higher than competing thermosets, the cost of the finished component can be roughly 20 to 40 percent lower due to reduced handling, processing and assembly costs. Thermoplastics also offer the option to fuse or weld molded subcomponents, which can reduce assembly weight and stress concentrations by eliminating fasteners and adhesives. Fig 1.3 shows the

timeline of the use of thermoplastic composites in commercial aircrafts, as per Fokker Aerostructures B.V.

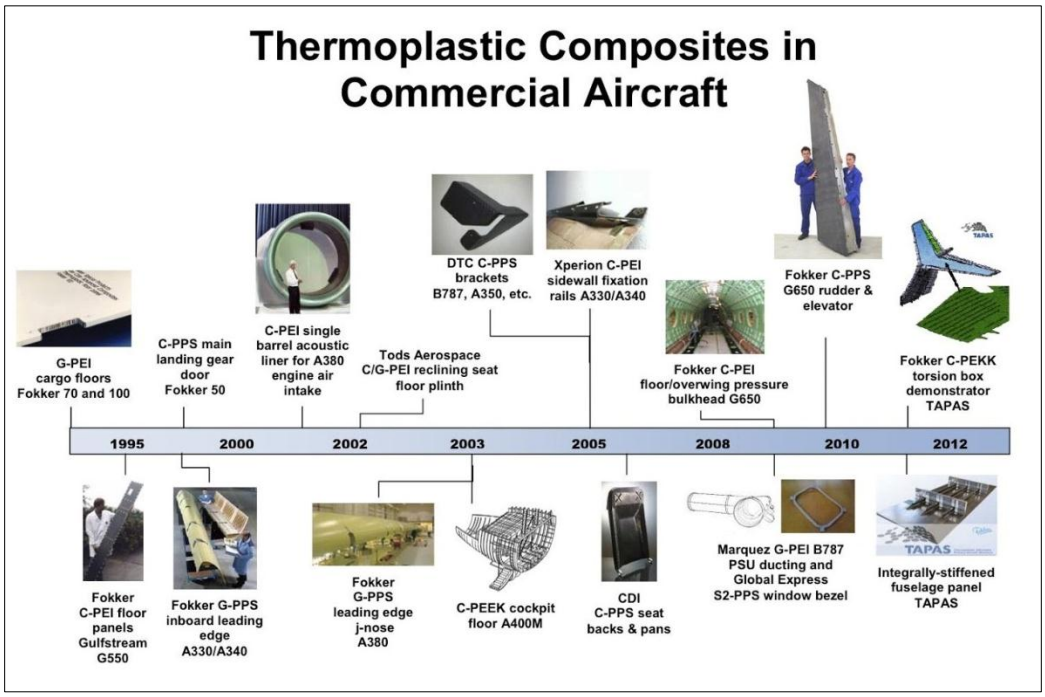

Figure 1-3 Thermoplastic Composites in Commercial Aircraft:

Now let us discuss the types of thermoplastics available and how they can be used as aircraft primary structures. With regard to high performance applications the early thermoplastics were insufficiently resistant to heat and moisture. The first high performance composites to become available had PEEK [4](Poly-Ether-Ether-Ketone) as a matrix. After this first step the need grew for a more affordable material that was easier to handle in production. PEI (Poly-Ether-Imide) [3]was next to be applied in structural parts. It was quite successful but it did have a drawback: it was sensitive to the kind of aggressive fluids that live in wide body aircraft. A better polymer had to be developed. With the year 2000 approaching this became PPS (Poly- Phenylene-Sulfide). No material is perfect for every application. PPS is widely

used, but its surface energy and shrinkage behaviour leave room for PEKK (Poly-Ether-Ketone-Ketone)[5]. Currently the most commonly used is the latest version of PPS, but the choice between PEEK, PEKK, PEI and PPS is fine-tuned to functional and process requirements. Affordability and weight are the determinant factors.

Table 1 summarizes the how the different thermoplastic composites stand based on various properties. Based on the ranking in this table, which was obtained by a report presented by Fokker Aerostructures, the right thermoplastic can be chosen for the right application.

Table 1-1 Comparison table for thermoplastic application

	Mechanical Properties	cost	processing temp	Tg	chemical resistance	bonding
PEEK	++	-	0	+	+	-
PEI	+	+	+	+	-	+
PPS	+	+	+	0	+	-
PEKK	++	0	0	+	+	+

1.3 PEKK Thermoplastic

As summarized by the table above, based on the required application a suitable thermoplastic polymer is chosen. For the current application, as explained in section 1.2. a material with high heat resistance, chemical resistance and the ability to withstand high mechanical loads is needed. Based on this need, the thermoplastic chosen for this research is PEKK (Poly-Ether-Ketone-Ketone)

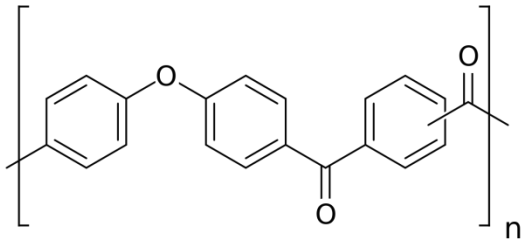

Figure 1-4 Chemical structure of Poly-Ether-Ketone-Ketone

Cytec Inc is one of key manufacturers of PEKK composites. PEKK consist of a matrix of poly(ether-ketone-ketone) polymer with aligned, continuous unidirectional fiber reinforcement. The composites have good structural performance at temperatures in excess of 250°F (121°C). PEKK composites can be used in lightly loaded applications at temperatures up to 400°F (204°C) due to the semi-crystalline nature of the polymer. PEKK composites possess outstanding flame, smoke and toxicity performance. They also have high toughness and damage tolerance.

Here are a few key features and benefit of PEKK thermoplastic

- Semi-crystalline, thermoplastic matrix
- Fully impregnated, unidirectional tape, ribbon and slit tape Tg of 318°F (159°C)*
- Service temperature of 257°F (125°C) for structural applications; up to 400°F (204°C) in certain applications
- Structural properties
- High toughness and damage tolerance
- Manufacture parts using affordable non-autoclave processes
- Outstanding FST1 and OSU2 heat release properties
- Good resistance to a wide range of fluid environments

- Low moisture uptake, < 0.3 wt%3
- Indefinite shelf life at room temperature
- Recyclable

Table 1-2 Physical Properties of PEKK thermoplastic

Property	*Room Temperature*
Shelf Life	Indefinate at 72 ^{o}F
Shop Life	Indefinate at 72 ^{o}F

Table 1-3 Neat Resin Properties

Property	*Room Temperature*
Density	1.310 g/cm^3 (% crystelline = 30%) 1.278 g/cm^3 (% crystalline = 0%)
Tg dry	318 ^{o}F
Tg wet	278 ^{o}F
Tm (melt point)	639 ^{o}F
Tensile Properties Strenght Modulus Elongation	 14.8 ksi (102 MPa) 0.65 Msi (4.5 Gpa) 4 %
Thermal Properties: Heat of Fusion With 100 % crystalline After cooling at 20 oC/min	 130 J/g 38.8 J/g
Flammability Properties Heat release rate (OSU, Peak/Total) Flammability Rating, UL-94 Limiting Oxygen Index	 <65 kW/m2 / <65 kW-min/m3 V-0 40

*Material Properties used while modeling

(https://www.cytec.com/sites/default/files/datasheets/PEKK_032012-02.pdf)

1.4 Fokker Aerostructures and TAPAS

Thermoplastic Primary Aircraft Structure innovation program (TAPAS), is a consortium that consists of companies and knowledge institutes in the Dutch aerospace industry working together with the aircraft manufacturer Airbus. The partners are jointly active in the aerospace industry, and work closely together with Airbus in the areas of materials, production and bonding technology and design. Development of the thermoplastic composites technology focuses on future Airbus applications, including primary structural components such as the fuselage and wings.[9] The partnership between Fokker Aerostructures and TenCate Advanced Composites with Airbus and the other partners started in 2010 and will run until end-2017. The Netherlands National Aerospace Laboratory (NLR), Delft University of Technology and the University of Twente are the Dutch partners in this innovation program.

Figure 1-5 The TAPAS 112m/39 ft- thermoplastic composite torsion box

As discussed in the previous sections, thermoplastic composites are advanced materials offering weight savings of 15% compared with traditional aircraft materials, together with benefits that include more efficient processing in production, lower costs of structural components and a high level of fire safety. These composites have

high strength, light weight and contribute to the drive towards sustainable aviation, because the use of these materials allows constant reductions in aircraft weight to be achieved. As a result fuel consumption is reduced, the range of the aircraft is increased and higher payloads are possible. The target is to further increase the proportion of thermoplastic composites in current aircraft as well as in the new generation of aircraft. A thermoplastic fuselage panel has been produced and presented as demonstrator as part of TAPAS 1. Currently, a demonstration tail section made entirely of thermoplastic composite material is being developed under the TAPAS 2 agreement. In the long term, the hope is to prove Thermoplastics as a viable option as a successor to a narrow body program.

1.5 PEKK Centre Beam - Problem Statement

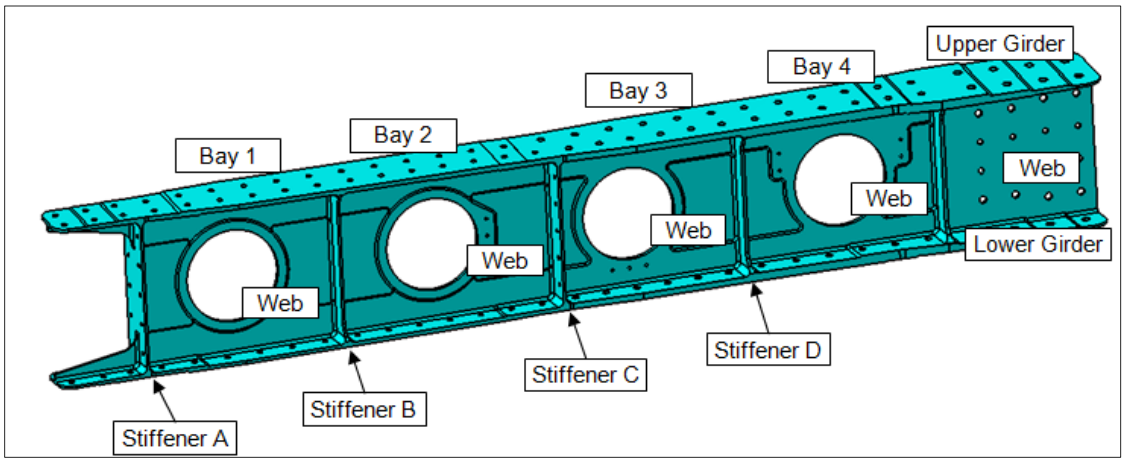

Figure 1-6 Centre Beam nomenclature of G650 aircraft

As a part of the TAPAS program, the collaborators intend to develop the technology necessary to produce large thermoplastic composite primary aircraft structures. The TAPAS torsion box is one of the structures being designed and analysed. The TAPAS torsion box demonstrator is basically a redesign of Gulfstream Aerospace Corp.'s

(Savannah, Ga.) Gulfstream G650 horizontal stabilizer, previously a carbon fiber/epoxy hat-stiffened skin construction. The torsion box is the fixed structure of the tail, and it is more heavily loaded than the movable rudder and elevators, which Fokker now produces in carbon/PPS, achieving a 10 percent weight reduction and a 20 percent cost savings vs. previous carbon/epoxy. The torsion box features tailored skins with varying thickness, from 2 mm/0.08 inch at its thinnest to 8 mm/0.4 inch at the root, and will be made from unidirectional carbon fiber/PEKK.

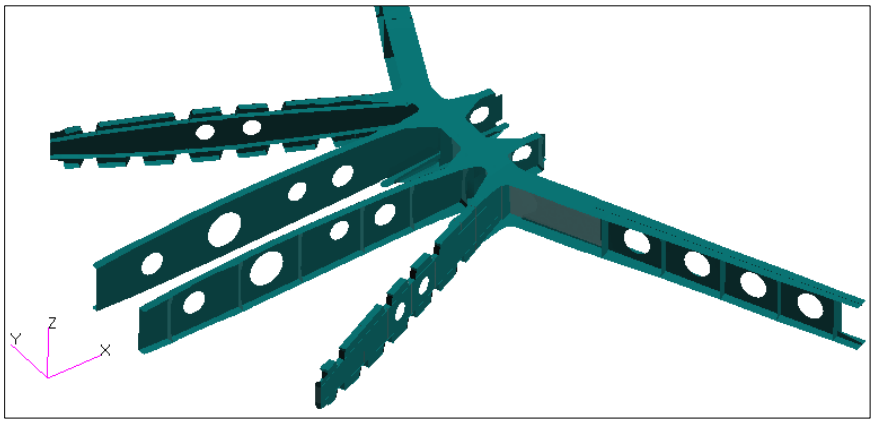

Figure 1-7 Beam, Rib1 And Root Rib Representation

For the purpose of this research, we will be with the loads acting on Section N of the center beam. The detailed FEM model used for the G650 analysis has been reused and adapted with the composite properties for the center-beam. Both the thermal and mechanical fastener loads are extracted from this model. The thickness and layups for the different bays and sections are given:

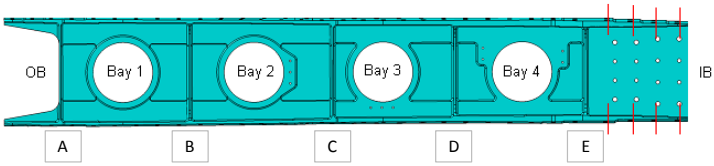

		Bay 1		Bay 2		Bay 3		Bay 4		Joints PF							
		G650	TAPAS	G650	TAPAS	G650	TAPAS	G650	TAPAS	G650				TAPAS			
Upper Flange t	[mm]	*4.80*	**4.97**	*5.55*	**6.07**	*7.10*	**8.00**	*9.81*	**10.21**	*9.70*	*7.50*	*5.00*	*2.70*	**8.00**	**6.62**	**4.97**	**4.97**
Web t	[mm]	*2.35*	**4.28**	*2.78*	**4.28**	*5.45*	**5.52**	*5.35*	**5.52**			*3.50*				**5.52**	
Lower Flange t	[mm]	*3.75*	**4.97**	*4.64*	**6.07**	*6.67*	**8.00**	*9.21*	**10.21**	*7.70*	*5.50*	*4.00*	*3.00*	**8.00**	**6.62**	**4.97**	**4.97**
Stiffener A	[mm]	*2.70*	**1.66**														
Stiffener B	[mm]			*2.70*	**2.07**												
Stiffener C	[mm]					*2.80*	**2.07**										
Stiffener D	[mm]							*3.40*	**2.21**								
Stiffener E	[mm]											*4.00*				**2.48**	

		Bay 1		Bay 2		Bay 3		Bay 4		Joints PF							
		G650	TAPAS	G650	TAPAS	G650	TAPAS	G650	TAPAS					TAPAS			
Upper Flange t	[# plies]		**36**		**44**		**58**		**74**					**58**	**48**	**36**	**36**
Web t	[# plies]		**31**		**31**		**40**		**40**						**40**		
Lower Flange t	[# plies]		**36**		**44**		**58**		**74**					**58**	**48**	**36**	**36**
Stiffener A	[# plies]		**12**														
Stiffener B	[# plies]				**15**												
Stiffener C	[# plies]						**15**										
Stiffener D	[# plies]								**16**								
Stiffener E	[# plies]														**18**		

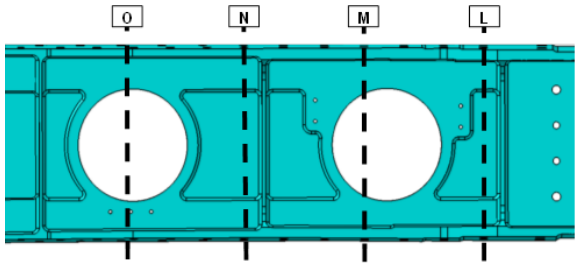

Figure 1-8 Centre beam section classification

Table 1-4 Geometry for Section N

Part	*Parameter*	*Dimension (mm)*
Flange	Plies	58
	Width	80
	Thickness	8.004
Web	Plies	40
	Width	175.4
	Thickness	5.52

According to data reported by Fokker Aerostructures, the load acting on the web, section N is 273 N/mm.

1.5.1 Objective of Project

There is a two-step objective for this Masters' research

1. Model the loading apparatus and the center beam in PEKK thermoplastic with a preexisting crack.
2. To apply the loads that is extracted from the G650 analysis and study the delamination, if any.

1.5.2 Scope of Project

The center beam is modeled as a uniform cross section I-beam, with the dimensions of the Rib3, Section N, using the composite layup provided in the previous section. A filler material is included between the flange and web as requested by Fokker Aerostructures. The loads are simulated by placing the I-beam under a four point bend experiment.

To analyze the delamination ABAQUS CAE is used, implementing two finite element methods: Virtual Crack Closure Technique (VCCT) and Cohesive Zone Method (CZM). The two methods are first validated by reproducing experimental data for calculating fracture toughness for PEKK Thermoplastic conducted by CYTEC Inc., for pure mode I and mode II delamination.

Finally, the C/PEKK I-beam is modeled in ABAQUS CAE, with an initial crack between the upper flange and filler. Under the four point bend test, the composite beam is subjected to mode II (or sliding mode) delamination. The delamination is analyzed using both virtual crack closure technique (VCCT) and cohesive zone method (CZM), to observe if there is crack propagation within the loads applied.

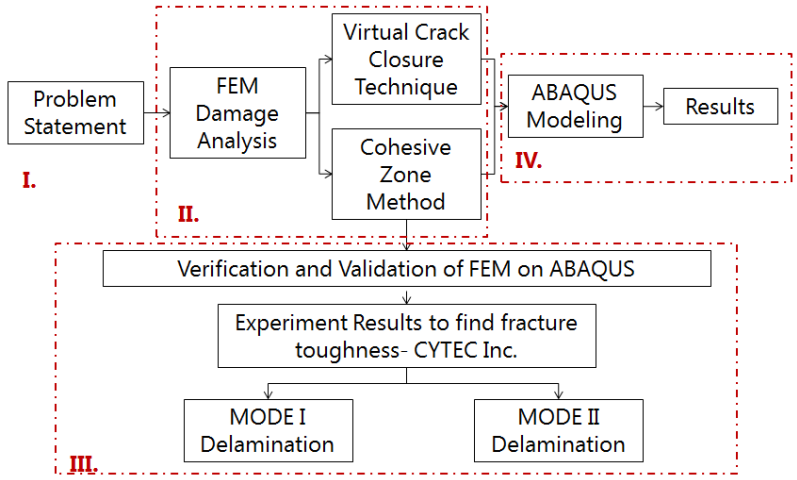

Figure 1-9 Scope of the Project

CHAPTER 2. FINITE ELEMENT APPROACHES FOR DAMAGE ANALYSIS

2.1 Finite Elemental Analysis for Delamination in Composites

Delamination, sometimes also called interlaminar cracking, is one of the most frequently encountered types of damage in advanced composite materials. In most cases, the delamination may often occurs due to poor bonding strength between adjacent layers depending merely on the polymer matrix. [10] Also, the defects and imperfections arising from the manufacturing process are also important factors leading to the deboning. In their paper, Sleight[11], Garnich and Akula Venkata [12], and Liu and Zheng [13] have given a review on the progressive failure analysis of composite laminates in terms of damage constitutive modeling by continuum damage mechanics and fracture mechanics.

Nowadays, the crack tip energy release rate (ERR) as a typical fracture parameter is widely used to predict the delamination crack propagation. [14] Mainly in the context of finite element analysis, the goal is to capture both the onset of delamination and its propagation. The procedures for numerical modeling of delamination can be divided into two main groups: (1) the models based on direct application of fracture mechanics, and (2) the models within the framework of damage mechanics. One of the most widely used fracture mechanics based approaches is the Virtual Crack

Closure Technique [15][16] (VCCT). This approach is based on Linear Elastic Fracture Mechanics (LEFM) and requires an initial crack to predict the delamination. Another widely used approach for modeling delamination based on damage mechanics is the cohesive elements based on the cohesive zone models [17][18]. A cohesive damage zone is assumed at the crack tip, and the model relates tractions to displacement jumps at an interface where a crack may take place. Both of these state-of-the-art methods have been incorporated into the ABAQUS® finite element software [19] for the simulation of initiation and extension of delamination.

2.2 Virtual Crack Closure Technique (VCCT)

2.2.1 Introduction

Delamination is the most commonly studied modes of failure in composites. Thus, fracture mechanics principles (Janssen et al., 2004) can be used to study the behavior of composite structures in presence of interlaminar damage and to identify the conditions when the forces start to propagate. Making the assumption that growth of delamination is the same as crack propagation[20][21], the science and mathematics of fracture mechanics can be used to study delamination as well. The propagation of a crack is possible when the energy released for unit width and length of fracture surface (named Strain Energy Release Rate, G) is equal to threshold level or fracture toughness, a physical characteristic for each material. Starting from the earlier analytical works by Chai et al.[22], and Kardomates[23][24] , delamination in composites has been studied by calculating the Strain Energy Release Rate at the

crack tip. Nowadays, the G calculation is generally performed by using finite element methods, such as the Virtual Crack Closure Technique.

From the definition mentioned above, the Energy Release Rate can be written as in Eq.(1).

$$G = lim\ \Delta a \to 0\ \frac{W}{\Delta a} \tag{1}$$

According to the Virtual Crack Closure Technique, the Strain Energy Release Rate is calculated based on the assumption that for an infinitesimal crack opening, the strain energy released is equal to the amount of the work required to close the crack. Inititally, the work *W* required to close the crack can be evaluated by performing two analyses. The first analysis is needed to evaluate the stress field at the crack tip for a crack of length *a* and the second one is aimed to obtain displacements in the configuration with the crack front appropriately extended from *a* to *a*+Δ*a*. However, today the method has been simplified to one step, by making a simple additional assumption: an infinitesimal crack extension has negligible effects on the crack front therefore both stress and displacement can be evaluated within the same configuration by performing only one analysis.

Thus, by adopting this technique, the expression of the work W required to close the crack becomes as in Eq. (2).

$$W = \frac{1}{2}\left[\int_0^{\Delta a} \sigma_{yy}^{(a)}(x)\, \delta u_y^{(a)}(x - \Delta a)dx + \int_0^{\Delta a} \sigma_{yx}^{(a)}(x)\, \delta u_x^{(a)}(x - \Delta a)dx + \int_0^{\Delta a} \sigma_{yz}^{(a)}(x)\, \delta u_z^{(a)}(x - \Delta a)dx\right] \tag{2}$$

where both displacements and stress are evaluated in the same configuration.

Now, combining the equation for the Energy Release Rate and the governing equation for One step- VCCT, (equations 1 and 2) it is possible to obtain the expression of the Strain Energy Release Rate for the three mutually orthogonal fracture modes: G_I , G_{II} and G_{III} that correspond to opening mode I, in-plane shear mode II and antiplanar shear mode III respectively.

2.2.2 Finite Element Implementation

As mentioned above, the state of delamination in a composite structure is determined by the comparing the Strain Energy Release Rate (G) with the fracture toughness (G_c) of the material, for a particular mode. We see a delamination only when the G numerically exceeds G_c . (Eq. 3)

$$G > G_c \tag{3}$$

However, for three orthogonal modes of loading, we have respective fracture modes defined. In a finite element model such as shown in Figure below, the energy released is the work done by the nodal forces required to close the crack tip, therefore:

$$G_I = \frac{1}{2b\Delta a} F_{cd}^{y}(v_c - v_d)$$

$$G_{II} = \frac{1}{2b\Delta a} F_{cd}^{x}(u_c - u_d)$$

$$G_{III} = \frac{1}{2b\Delta a} F_{cd}^{yz}(w_c - w_d) \tag{4}$$

where *b* is the specimen thickness, *F* corresponds to the magnitudes of nodal forces pairs at nodes c and d in the y, x and z direction, respectively. *u* and *v* are the nodal displacement before nodes c and d are pulled together.

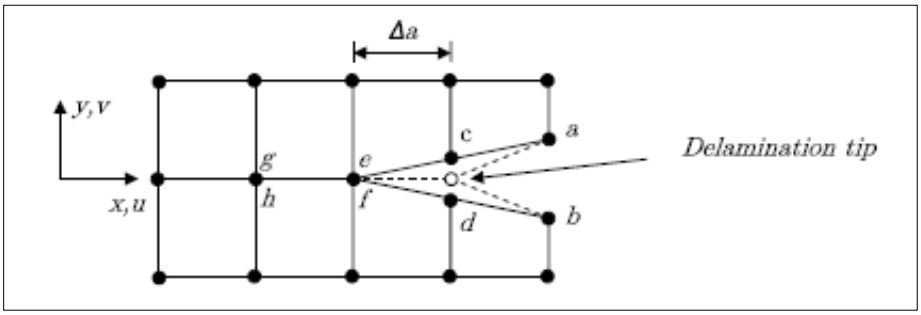

Figure 2-1 Calculation of the energy release rate using Virtual Crack Closure technique

After the calculation of G_I, G_{II} and G_{III}, the total energy release rate reads

$$G_T = G_I + G_{II} + G_{III}$$

As mentioned before, delamination begins when the computed energy release rate is equal to the fracture toughness, G_c

$$G_T = G_c$$

One advantages of this form of calculation is that it is based on energy rather than stress.

2.3 Cohesive or Damage Zone Models (CZM)

2.3.1 Introduction

Another approach for the numerical simulation of the delamination can be developed within the framework of Damage Mechanics. Model formulated using Damage Mechanics are based on the concept of the cohesive crack model: a cohesive Damage Mechanics are based on the concept of the cohesive crack model: a cohesive damage zone is developed near the crack front.

Cohesive damage zone models relate traction forces in the defined cohesive zone to displacement discontinuities at the crack tip. Damage initiation depends on the maximum value of the traction forces, in the traction-displacement curve (T-Δ). When the area under the traction-displacement graph is equal to the fracture toughness Gc, the traction is reduced to zero and new crack surfaces are formed.

The advantages of the CZM approach are its unification of crack initiation and growth into one model. Cohesive zone model formulations are more powerful than fracture mechanics because they allow the prediction of both initiation and crack propagation. The formulation and finite element implementation is described below.

In the simplest and most usual formulation of CZM, the entire body under consideration is assumed to be linear elastic, while the area in the cohesive zone is embedded with the non-linear cohesive law (Fig. 2.3). The cohesive law dictates the interfacial law that acts on the crack line. The stress in the cohesive law is the cohesive strength of the material, σ_c, while the area under the curve is the cohesive fracture energy, G_c. The entire fracture process can be summarized in Fig. 1: In stage 1, the linear elastic behavior of the model, as mentioned in the assumption, prevails. As the load increases at the crack front, the crack initiates (2). The region with 2 and 3 is the area governed by the cohesive law, which in nonlinear and grows from initiation to full failure. At 4, when the area under the area under the curve equals the fracture toughens, a new traction free surface appears ($\Delta=\Delta c$).

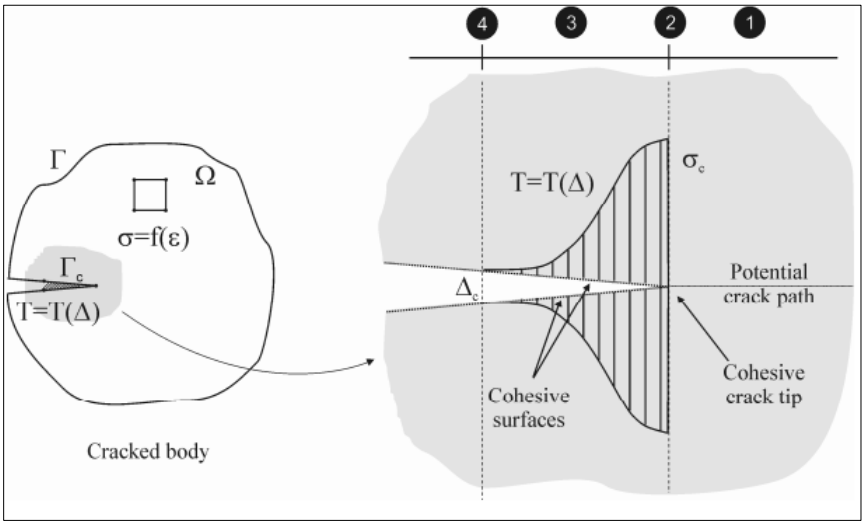

Figure 2-2 Cohesive zone modeling of fracture

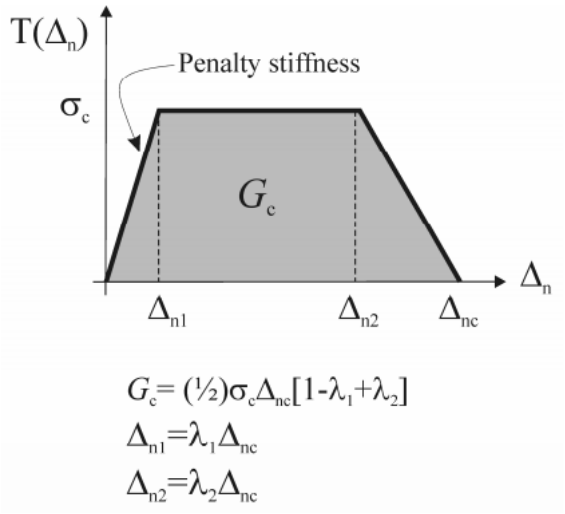

Figure 2-3 Cohesive Law

Therefore, the continuum should be characterized by two constitutive laws; for instance, a linear stress-strain relation for the bulk material and a cohesive surface relation (cohesive law) that allows crack spontaneous initiation and growth.

Now we discuss the finite element implementation of cohesive zone models. The cohesive view of fracture is captured by surface constitutive relations that describe the evolution of tractions (T) generated across the faces of a crack as a function of the crack face displacements jump (Δ). Therefore, implementation of cohesive zone in FEM framework requires bulk finite elements, for modeling the stage (1) in Fig. 2.3, bordered by cohesive surface elements for the remaining three stages: (2) crack initiation, (3) crack evolution and (4) complete failure. The insertion of cohesive surface elements bridges linear elastic and fracture behavior allowing for spontaneous crack propagation.

2.3.2 Finite Element Implementation

In the cohesive zone model fracture is captured by relations that describe the evolution of tractions (T) generated across the faces of a crack as a function of the crack face displacements jump (Δ). Therefore, implementation of cohesive zone in FEM framework requires bulk finite elements, for modeling the stage (1) in Fig.2.3, bordered by cohesive surface elements (2) crack initiation, (3) crack evolution and (4) complete failure. The principle of virtual work including the contribution of cohesive surfaces is given as follows

$$\int_{\Omega} \sigma : \varepsilon \, d\Omega - \int_{\Gamma_c} T \cdot \Delta_n \, d\Gamma_c - \int_{\Gamma} P \cdot u \, d\Gamma = 0 \qquad (5)$$

Where ε is the virtual strain associated to the virtual displacement u defined in the domain Ω; Δ_n is the virtual crack faces normal displacement jump along the crack line Γ_c; T is the traction vector along the cohesive zone; P is the external traction vector (see Fig.1). The first term in Eq. (1) is the internal virtual work for bulk elements

while the contribution of cohesive surface elements to the internal virtual work is represented by the second integral. Exploiting the finite element formulation, we can rewrite Eq. 8 as

$$\left[\int_{\Omega} B^T EB d\Omega - \int_{\Gamma_c} N_c^T \quad \frac{\partial T}{\partial \Delta_n} N_c d\,\Gamma_c\right] d = \int_{\Gamma} N^T P\, d\Gamma \tag{9}$$

Where N and N_c are matrices of the shape functions for bulk and cohesive elements, respectively, B is the derivative of N, d are the nodal displacements, E is the tangential stiffness matrix for the bulk elements, and $\partial T/\partial \Delta_n$ is the Jacobian stiffness matrix. Therefore, in order to carry out the iterations of the method [19], the contribution of cohesive elements to the tangent stiffness matrix as well as to the force vector is acquired from the numerical implementation of the CZM**.**

2.4 Virtual Crack Closure Technique v/s Cohesive Zone Modeling

Here is a brief summary of each methods strengths and weaknesses

Cohesive Zine Modeling: relates interfacial tractions to displacement discontinuities.

Strength

- Predicts initiation and growth of delamination without prior assumptions about the crack.
- Applicable to complex structures subjected to complex loading states.

Weaknesses

- Characterization data can be difficult to obtain.
- Accurate assessments are strongly tied to element size.

Virtual Crack Closure Technique: calculates energy-release rate, with the assumption that the energy needed to separate a surface is the same as the energy needed to close the same surface.

Strength

- Mature fracture mechanics-based technique with a large body of work.
- The growth criteria is the energy release rate, G.

Weakness

- Assumptions about cracks must be made (number, location, size)
- Can be difficult to incorporate for complex structures and loading.

CHAPTER 3. VALIDATION OF FE METHODS USING ABAQUS CAE

3.1 Three modes of Crack Extension

Delamination fracture may occur in three different loadings, referred to as opening or peel mode (mode I), forward sliding shear mode (mode II), and tearing mode (mode III). As shown in figure 3.1 these modes are based on the loading condition and relative displacements of the crack faces. The resistance to delamination growth is expressed in terms of delamination fracture toughness, which is generally measured experimentally. Numerous studies have attempted to determine delamination criterion based on the resistance to delamination due to mixed-loadings by combination of pure modes [29].

For this thesis research, the two methods mentioned in Chapter 2 are verified and validated using the experimental results provided Cytec Inc. for PEKK thermoplastic polymer. The experiments are simulated based on the ASTM standards for pure mode I and II. The experimental data was provided to Fokker Aerostructures as part of the TAPAS program.

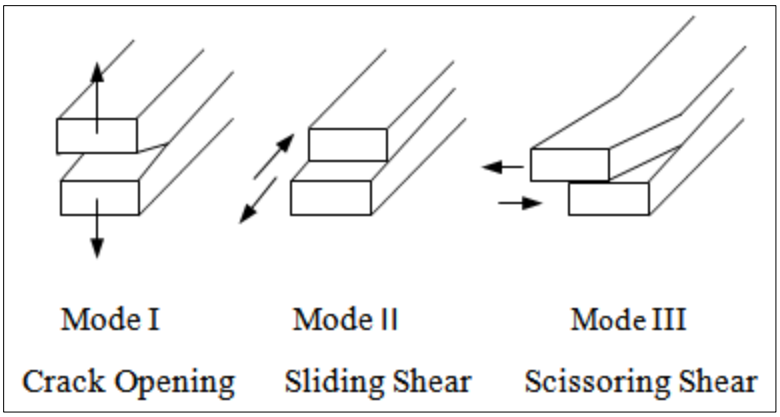

Figure 3-1 Three modes of delamination in composite structures

3.2 MODE I Delamination

Mode 1 delamination also knows as the opening or peel mode. To determine the Mode I interlaminar fracture toughness G_{IC} of a fiber-reinforces composite material, ASTM has defined a standard experimental procedure using a double cantilever beam; ASTM D5528 '*Standard Test Method for Mode 1 Interlaminar Fracture Toughness of Unidirectional Fiber-Reinforced Polymer Matrix Composites*'.

This test method is limited to use with composites consisting of unidirectional carbon fiber and glass fiber tape laminates with brittle and tough single-phase polymer matrices. The energy release rate G, which is defined as the loss of energy, dU, in the test specimen per unit of specimen width for an infinitesimal increase in delamination length, *da*, for delamination growing under a constant displacement, can be mathematically represented as

$$G = -\frac{1}{b}\frac{dU}{da}$$

Where U is the total elastic energy in the test specimen, b is the specimen width and *a* is the delamination length. Fig 3.1 describes the experimental set up for the ASTM D5528.

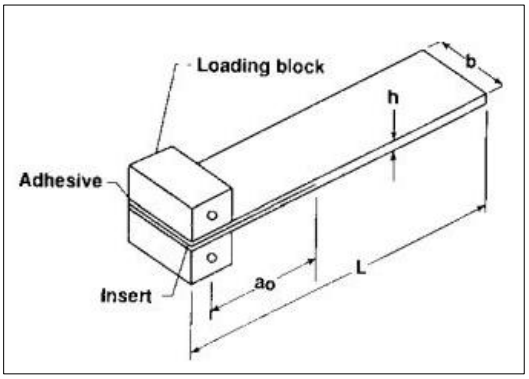

Figure 3-2 Double cantilever beam specimen with loading blocks

3.2.1 Experimental Test Method and Cytec results

The DCB shown in Fig 3.1 consists of a rectangular, uniform thickness, unidirectional laminated composite specimen containing a non adhesive insert of the midplane that serves as a delamination initiation. Opening forces are applied to the DCB specimen by means of the loading blocks bonded to one end of the specimen. The ends of the DCB are opened by controlling either the opening discplacement or the crosshead movement, while the load and delamiantion lengtha are recorded.

A record of the applied load versus opening displacement is recorded on an *X*-*Y* recorder or equivalent real-time plotting device or stored digitally and post-processed. Instantaneous delamination front locations are marked on the chart at intervals of

delamination growth. The Mode I interlaminar fracture toughness is calculated using a modified beam theory or compliance calibration method.

The brief procedure for the experimented is given below according to the ASTM description.

1. Measure the width and thickness of each specimen and the average values of the width and thickness measurements shall be recorded.
2. Mark the first 5 mm from the insert for every 1 mm. Mark the remaining 20 mm with thin vertical lines every 5 mm.
3. Mount the load blocks or hinges on the specimen in the grips of the loading machine, making sure that the specimen is aligned and centered.
4. As load is applied, measure the delamination length, *a*, on one side of the specimen. The initial delamination length, a_0, is the distance from the load line to the end of the insert.

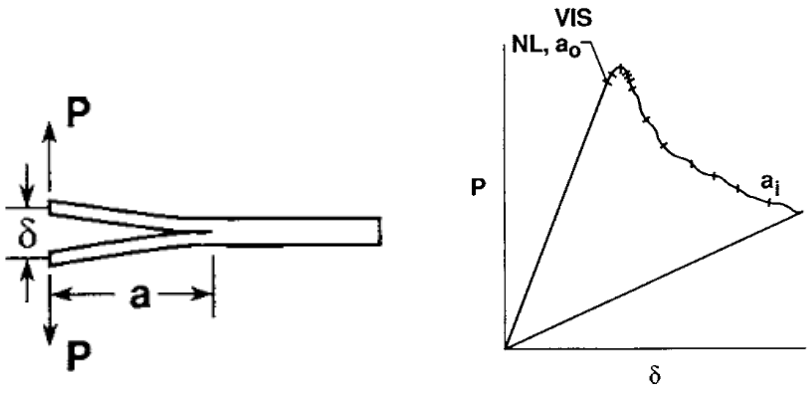

Figure 3-3 Load displacement trace from DCB test for Mode I

Load the specimen as a constant crosshead rate between 1 and 5 mm/min. Record the load and the displacement values, continuously. During loading, record the point on

the load-displacement curve as can be seen Fig 3.3., values at which the onset of delamination movement from the pre-crack is observed on the edge of the specimen (VIS, Fig 3.3).

Cytec followed the above procedures with four specimens as mentioned above. The physical properties of the four specimens are mentioned in Table 3.1.

Table 3-1 CYTEC Inc. sample specimen

Specimen No.	Width (mm)	Thickness (mm)	Cured Ply Thickness (mm)	No of plies	Pre-Crack length, a_0 (mm)
1	25.5	4.29	0.143	30	57.0
2	25.5	4.24	0.141	30	57.7
3	25.5	4.22	0.140	30	56.7
4	25.5	4.23	0.141	30	57.3
Average	**25.5**	**4.24**	**0.141**	**30**	**57.17**

The load-vs displacement graph for the PEKK thermoplastic for the DCB test is given below in Fig 3.4

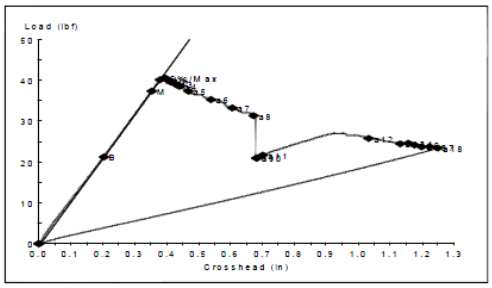

Specimen 1

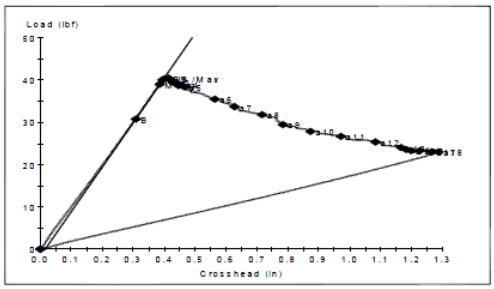

Specimen 2

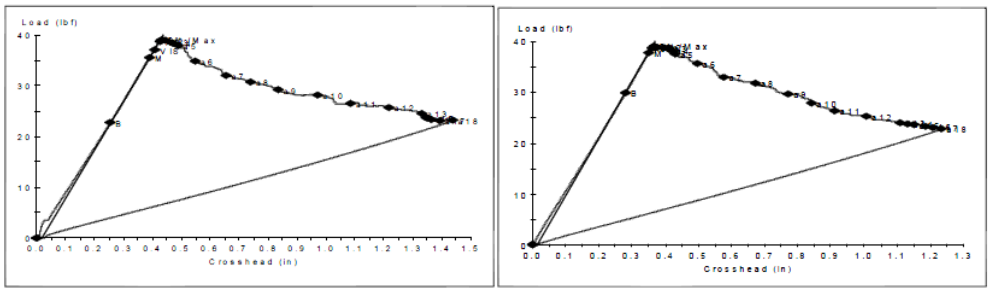

Specimen 3 Specimen 4

Figure 3-4 Load v/s cross-head displacement for the four specimens

The calculation of the interlaminar fracture toughness, G_c, can be done in multiple ways. These consist of a modified beam theory (MBT), a compliance calibration (CC) and a modified compliance calibration method (MCC).

For this research, to validate the VCCT and the cohesive element plug in ABAQUS CAE, the Load v/s cross head displacement graph will be replicated.

3.2.2 ABAQUS CAE Model

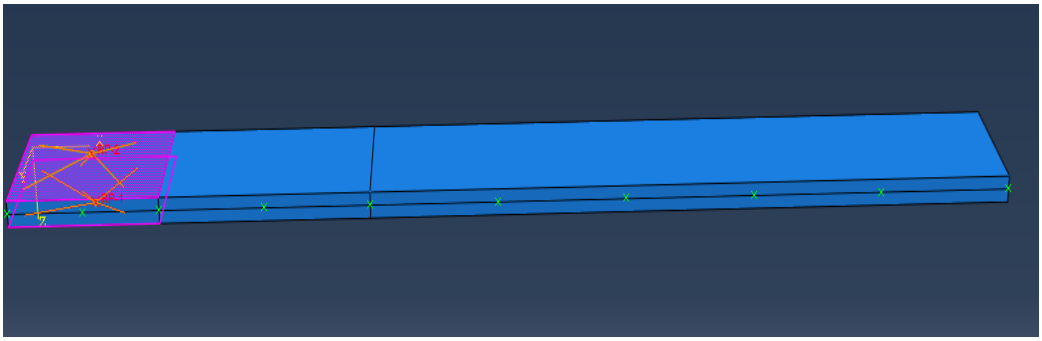

Figure 3-5 Modeling ASDM 5528 on Abaqus CAE

Table 3-2 Physical Dimensions of the model

Property	*Magnitude*	*Unit*
Length	200	mm
Width	25.4	mm
Ply Thickness	0.138	Mm
No of Plies	30	-
Layup	$[0]_{30}$	-
Initial delamination, a_o	57	mm

Table 3-3 C/PEKK Material Properties

Property	*Value*	*Unit*
E_1	133450	N/mm^2
E_2	10800	N/mm^2
E_3	5460	N/mm^2
ν_1	0.319	
ν_2	0.319	
ν_3	0.02	
G_{12}	5460	N/mm^2
G_{13}	5460	N/mm^2
G_{23}	5088	N/mm^2
Ply Thickness	0.138	mm

3.2.3 Constraints and Boundary Conditions

There are two constraints acting on this model, and they are to simulate the loading blocks as shown in Fig 3. The loading pins aren't physically modelled but are simulated by coupling the contact surfaces with a reference point. These reference points control the displacement and forces, and the boundary conditions are applied to them.

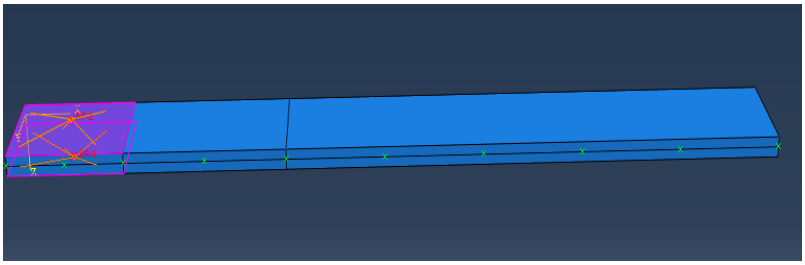

Figure 3-6 Coupled surfaces to simulate Loading Pins

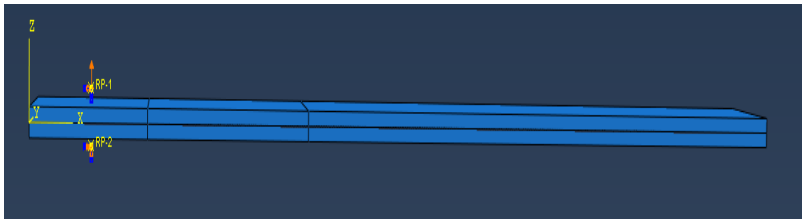

Figure 3-7 Boundary Conditions applied to reference points

As mentioned above, boundary conditions are applied to the reference points, which is a constant displacement loading as described in the table below.

Table 3-4 Boundary conditions acting on model

Reference Point	U_1	U_2	U_3
1 (top)	0	0	33 mm
2 (bottom)	0	0	0

3.2.4 Interactions

Interactions acts are defined between the two surfaces in contact. There are two separate set of interaction s acting for this research; VCCT and CZM. The specifications for these interactions are defined in the next section.

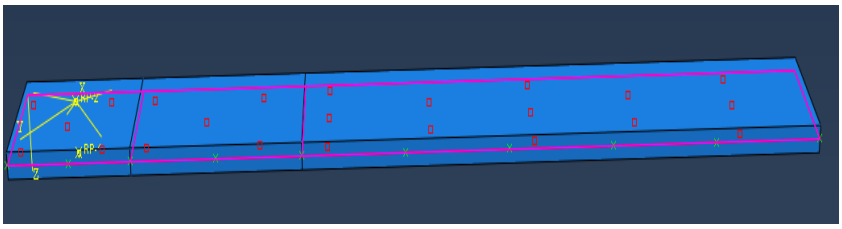

Figure 3-8 Mid-plane interactions on the DCB

The mid plane of the beam is interacting via two defined surfaces: the Master surface and the Slave surface. The initial delamination is created by a node set which represents the initially bonded area.

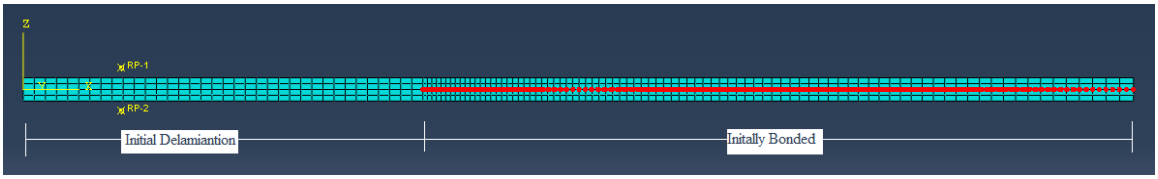

Figure 3-9 Initially bonded and unbonded region

3.2.4.1 VCCT Interaction

The following interactions are acting when the VCCT delamination criteria is in place.

Table 3-5 VCCT Interaction Properties

Interaction	*Specifications*
Tangential Behavior	Frictionless

Normal Behavior	Pressure Behavior = Hard contact				
Fracture Criterion: VCCT	Critical Energy Release Rate	Mode I = 1.5	Mode II = 4.7	Mode III = 4.7	Exponent = 1.75

3.2.4.2 CZM Interaction

Table 3-6 CZM Interaction Properties

Interaction	*Specifications*			
Tangential Behavior	Frictionless			
Normal Behavior	Pressure Behavior = Hard contact			
Cohesive Behavior	Traction-Separation Behavior	K_{nn} = 1e6	K_{ss} = 1e6	K_{tt} = 1e6
Damage	Initiation (Maximum Nominal Stresses)	Normal = 80	$Shear_1$ = 122	$Shear_2$ = 122
	Evolution (Linear Energy following	Normal Fracture Energy = 1.35	$Shear_1$ Fracture Energy = 5	$Shear_2$ Fracture Energy = 5

	Benzeggagh-Kenane Law) BK Exponent = 1.45			

3.2.5 RESULTS

3.2.5.1 VCCT Mode I

After application of loads, the crack propagates along the designated crack path. The final results, after delamination, look like the figure below.

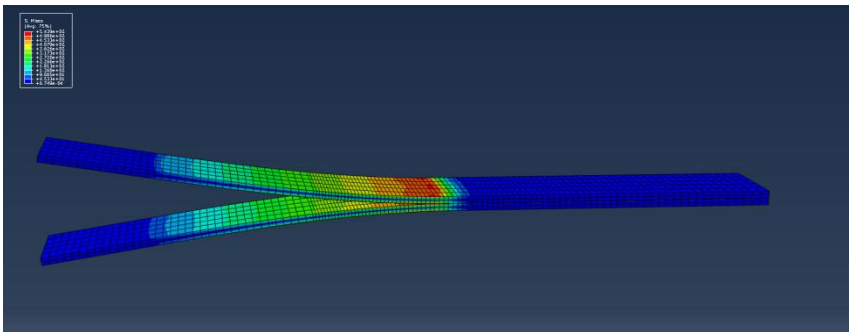

Figure 3-10 Delamination from VCCT interaction

The beam starts delaminating when the load corresponds to 163.686 N and the cross-head displacement, or the opening distance is 9.384 mm

3.2.5.2 Cohesive Zone Method Mode I

Using the cohesive surfaces predicts crack propagation too. Here, the delamination starts growing when the load on the loading pins reaches 162.232 N and the cross head displacement is 9.575 mm.

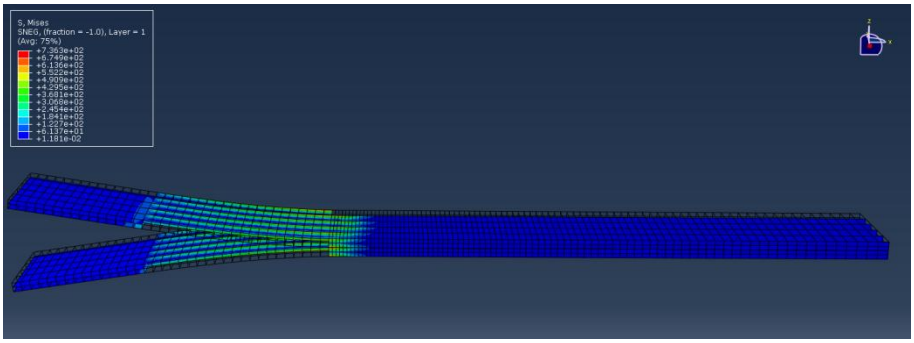

Figure 3-11 Delamination from VCCT interaction

3.2.6 Observations and Validation

The results obtained by both the VCCT model and the CZM model have to be validated, in order to proceed further. This validation is done by comparing the load-displacement graph that was provided by Cytec Inc. The load corresponds to the forces acting on the loading pins on the Double Cantilever Beam, and the displacement corresponds to the crosshead displacement between the opening ends of the beam. The results are plotted in the figure below

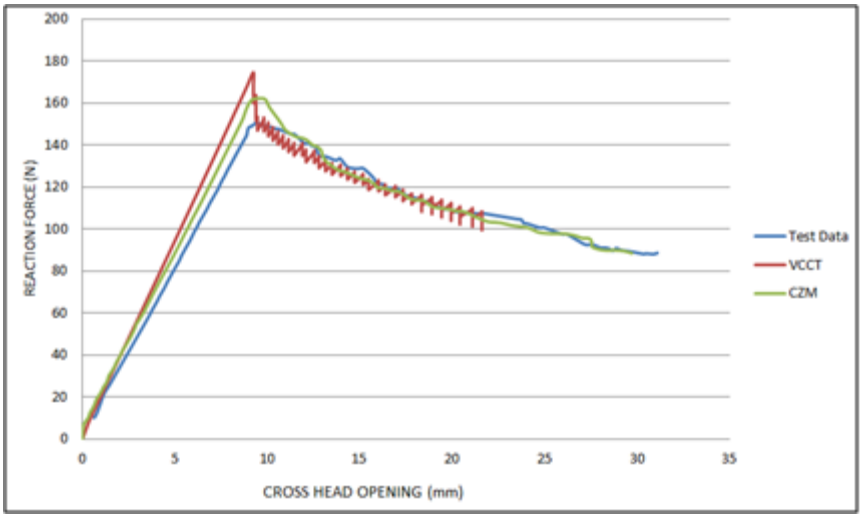

Figure 3-12 Load-Displacement graph of the DCB mode 1

Thus, as we can see from the results, the graph plotted by ABAQUS, is similar to that provided by CYTEC. The peak loads, that correspond to when the crack starts propagating, and their corresponding crosshead displacements are mentioned in the table below.

Table 3-7 Summary of delamination results

MODEL NAME	*PEAK LOAD (N)*	*CROSS HEAD DISP. (mm)*
Test Data by CYTEC Inc.	150.5	9.4
Analysis with VCCT	163.6	9.3
Analysis with CZM	162.2	9.5

3.3 Mode II Delamination

Mode II crack extends as a result of shear forces at the crack tip, hence giving it the name 'Sliding Mode'. To calculate the fracture toughness energy G_{IIC}, the standard procedure is subscribed by the European Association of Aerospace Industries (AECMA) under prEN 6034 "*Carbon fibre reinforced plastics test method- Determination of interlaminar fracture toughness energy Mode II, G_{IIC}*"

The end notched flexure specimen is used for this testing. A precracked specimen is loaded in a three point bend fixture, as shown in Fig 3.4 until crack propagation onset. The load applied to the specimen and the cross-head displacement of the test machine is recorded continuously during the test. The total fracture toughness energy is calculated from the crack length and load- displacement diagram.

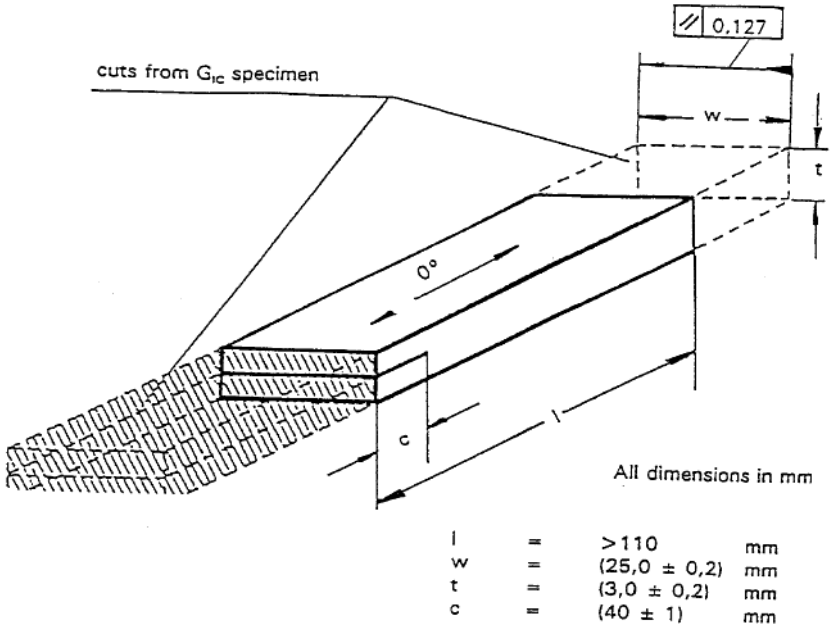

Figure 3-13 Standard test specimen for EN6034

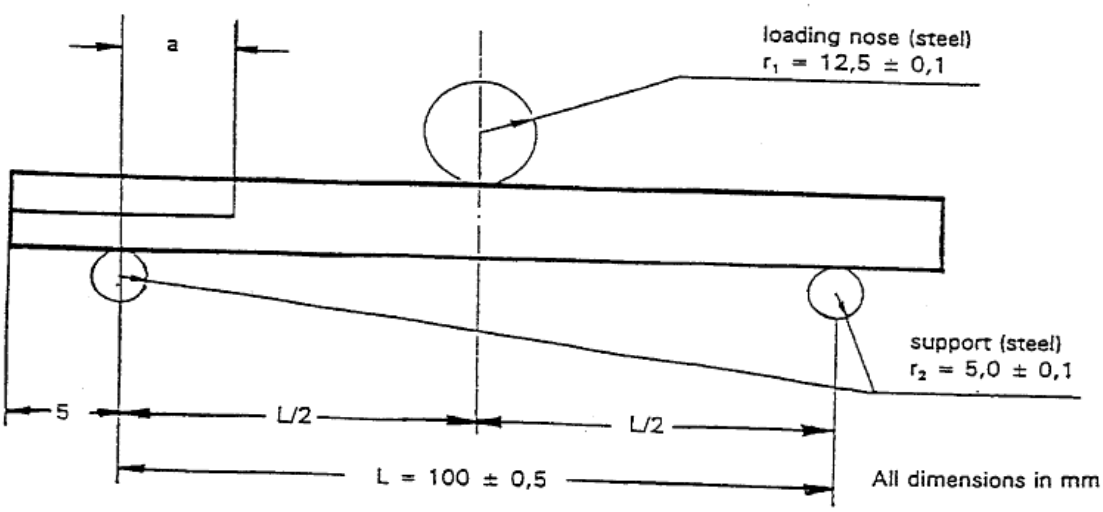

Figure 3-14 Test fixture

3.3.1 Experimental procedure and Cytec Results

To achieve reproducible test results, the procedure as specified on pEN6034 has to be followed. The initial crack lengths must be accurately measured and the continuous

load-displacement record must be made, measuring the displacement of the loading nose.

The following procedure shall then apply;

- Adjust load cell reading and displacement reading to 0
- Load the specimen under the displacement control at a rate of 1 mm/min
- Optically observe the crack tip to detect the crack propagation onset
- Record critical load at the delamination crack onset and stop the loading as soon as evidence of crack propagation has confirmed by a small load drop.

To calculate $G_{IIC,}$ the following formula is used

$$G_{IIC} = \frac{9000\ P\ a^2\ d}{2w\left(\frac{1}{4}L^3 + 3a^3\right)}$$

Where

G_{IIC} is the fracture toughness energy in J/m^2, d is the cross head displacement at the crack delamination onset, P is the critical load, *a* the initial crack length, w and l are the width and span length respectively.

To calculate the fracture toughness, CYTEC Inc. followed the procedure mentioned with four specimens.

Table 3-8 Cytec Inc. specimen specifications

Specimen	*Width (mm)*	*Thickness (mm)*	*Initial Crack length (mm)*	*Span Length (mm)*	*Critical Start Load (N)*	*Peak Load (N)*	*G_{IIC} (J/m^2)*
1	25.0	4.351	35	100	2182.6	2256.2	5667.6
2	25.1	4.359	35	100	2219.1	2247.4	5656.1
3	25.1	4.351	35	100	2103.2	2122.9	4884.2
4	25.0	4/354	35	100	1914.6	1957.2	4229.5

With the specimen mentioned above, the following load-cross head displacement graph was obtained.

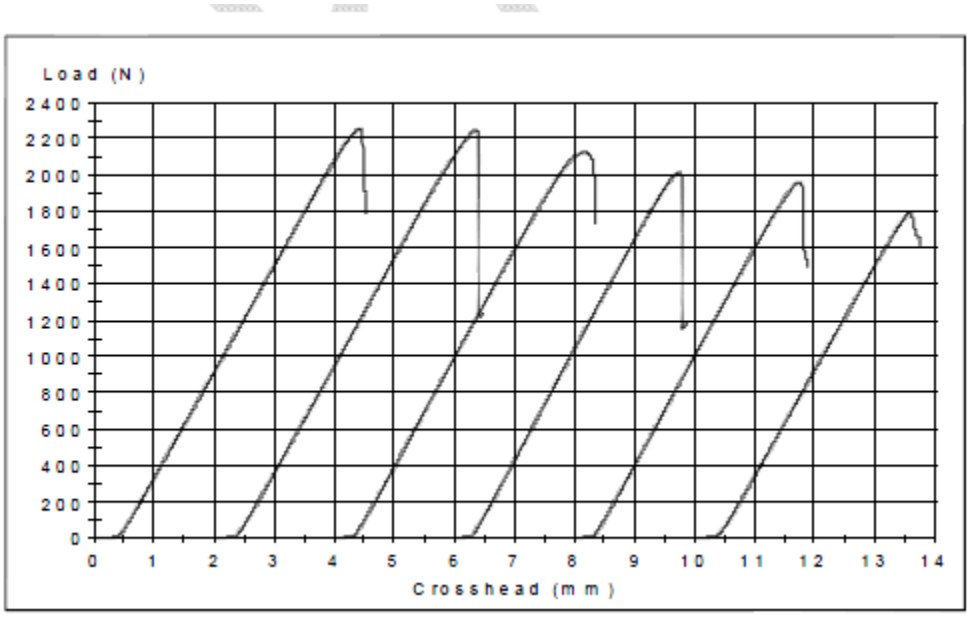

Figure 3-15 The load-displacement graph provided by Cytec

3.3.2 Abaqus CAE Model

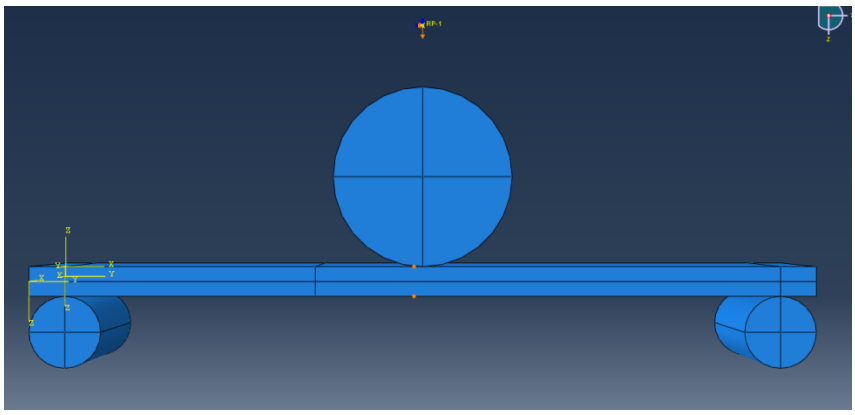

Figure 3-16 Abaqus CAE model for EN 6034

The above figure shows the ABAQUS model of the Mode II delamination set up. The set up consists of four parts: The central beam, with the delamination, two support beams and the loading pin. The beam is made of C/PEKK thermoplastic and the pins from steel.

Table 3-9 Physical properties of the model

Property	*Value*	
Length	110	mm
Width	25	mm
Ply Thickness	0.138	mm
# Plies	30	-
Layup	$[0]_{30}$	-
Initial Delamination	35	mm
Loading Pin diameter	25	mm
Support Pin diameter	10	mm

3.3.3 Material Properties

Table 3-10 C/PEKK Thermoplastic

Property	*Value*	*Unit*
E_1	133450	N/mm^2
E_2	10800	N/mm^2
E_3	5460	N/mm^2
ν_1	0.319	
ν_2	0.319	
ν_3	0.02	
G_{12}	5460	N/mm^2
G_{13}	5460	N/mm^2
G_{23}	5088	N/mm^2
Ply Thickness	0.138	mm

Table 3-11 Steel (Loading/Support Pins)

Property	*Value*	*Unit*
E_1	133450	N/mm^2
ν_1	0.319	

3.3.4 Boundary Conditions and Constraints

The three pins are modelled as rigid bodies that are controlled by a corresponding reference points. These reference points are then given a boundary condition.

The support pins are grounded, that is all their degrees of freedom are restricted. The loading pin is given a displacement loading of -13 mm along the z direction, while the others are restricted to avoid rotation.

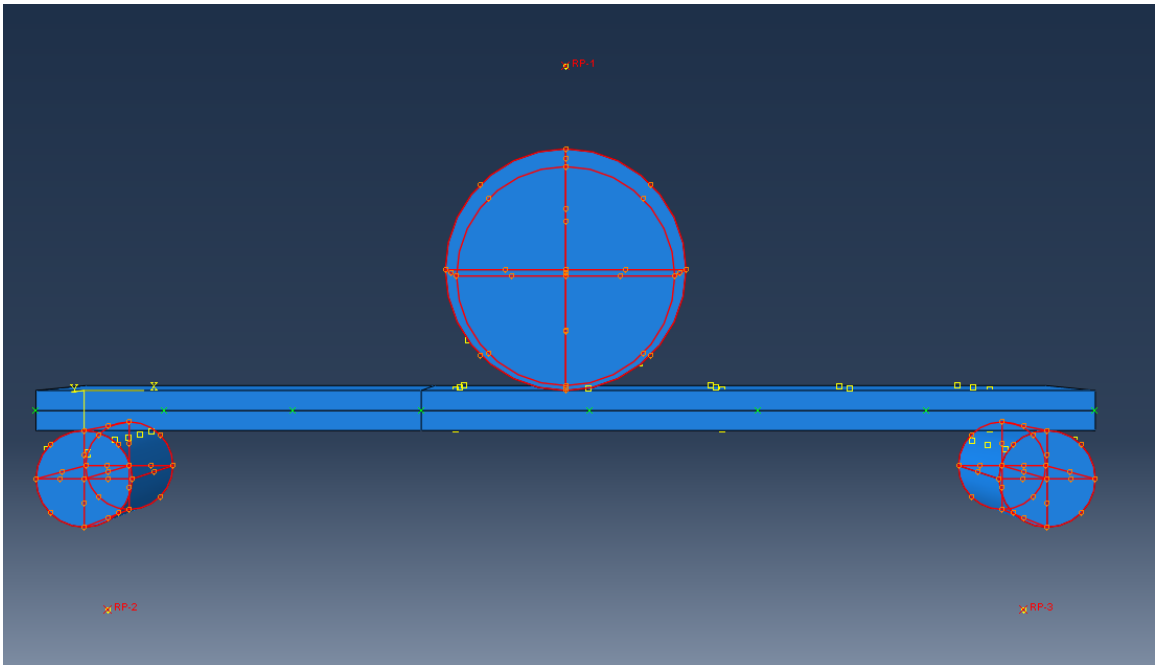

Figure 3-17 Support and Loading Pins modeled as rigid bodies

Table 3-12 Boundary Conditions for Mode II delamination setup

Reference Point	*U1*	*U2*	*U3*
1 (loading)	0	0	-13
2 (support)	0	0	0
3 (support)	0	0	0

3.3.5 Interactions

Interactions are inserted mid-plane in the beam, where the pre crack lies and the crack will propagate. This interaction can be VCCT or CZM, with the same properties as mentioned in the previous section.

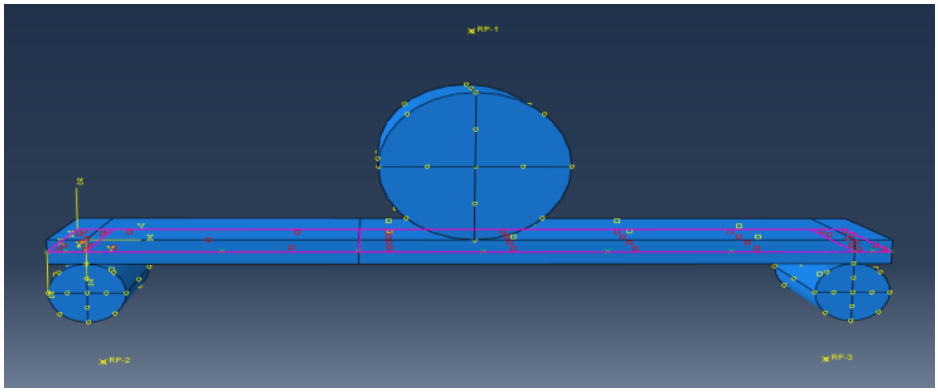

Figure 3-18 Mid-plane interaction mode II

The pre crack is again defined by a set of nodes that are initially defined as ‘bonded’. The nodes not part of this set constitute the initial delamination, 35 mm.

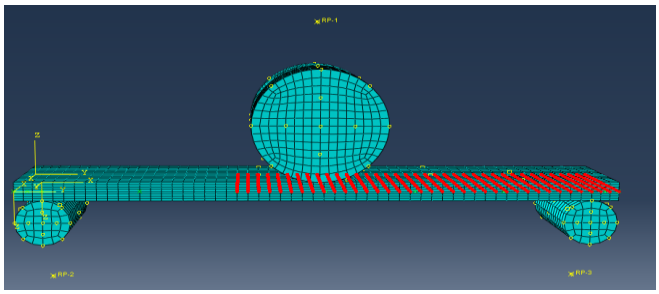

Figure 3-19 Initial delamination mode II

3.3.6 Results

On application of displacement loading, the beam ends resulting in Mode II delamination. However, according to the procedure the displacement is stopped as soon as the crack starts to propagate. This was followed while following the VCCT model, but for CZM model, the displacement was continued to see the graph. The final results are shown below along with the load-displacement graphs.

3.3.6.1 VCCT Model

After application of loads, the crack propagates along the designated crack path. The final results, after delamination, look like the figure below.

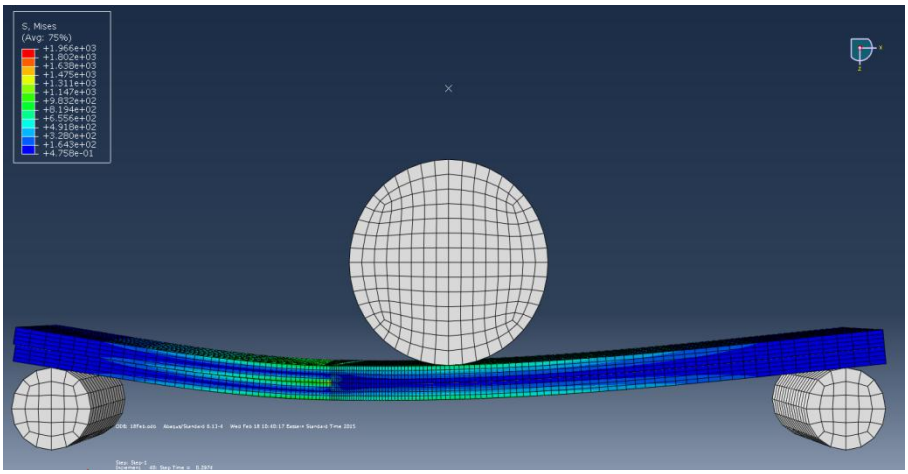

Figure 3-20 Final mode II deformation VCCT

The beam starts delaminating when the load corresponds to 2386.46 N and the cross-head displacement, or the opening distance is 3.75 mm

3.3.6.2 Cohesive Zone Model

Using the cohesive surfaces predicts crack propagation too. Here, the delamination starts growing when the load on the loading pins reaches 2000.6 N and the cross head displacement is 3.69 mm.

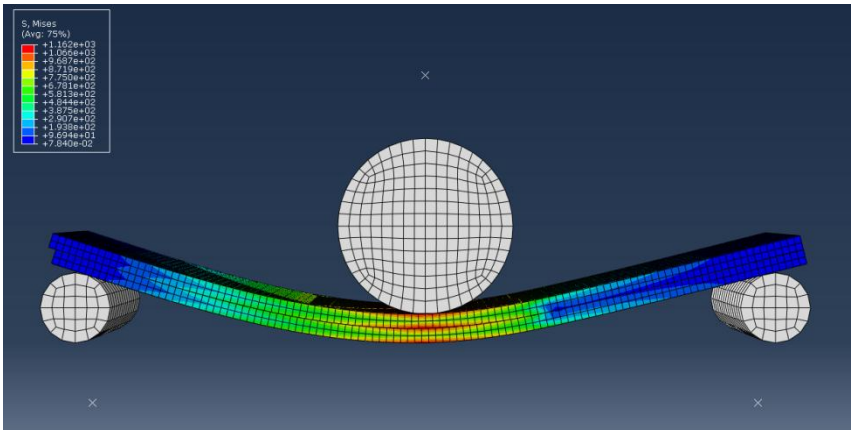

Figure 3-21 Final mode II deformation VCCT

3.3.7 Observations and Comparison

The results obtained by both the VCCT model and the CZM model have to be validated, in order to proceed further. This validation is done by comparing the load-displacement graph that was provided by Cytec Inc. The load corresponds to the forces acting on the loading pins on the Double Cantilever Beam, and the displacement corresponds to the crosshead displacement between the opening ends of the beam. The results are plotted in the figure below

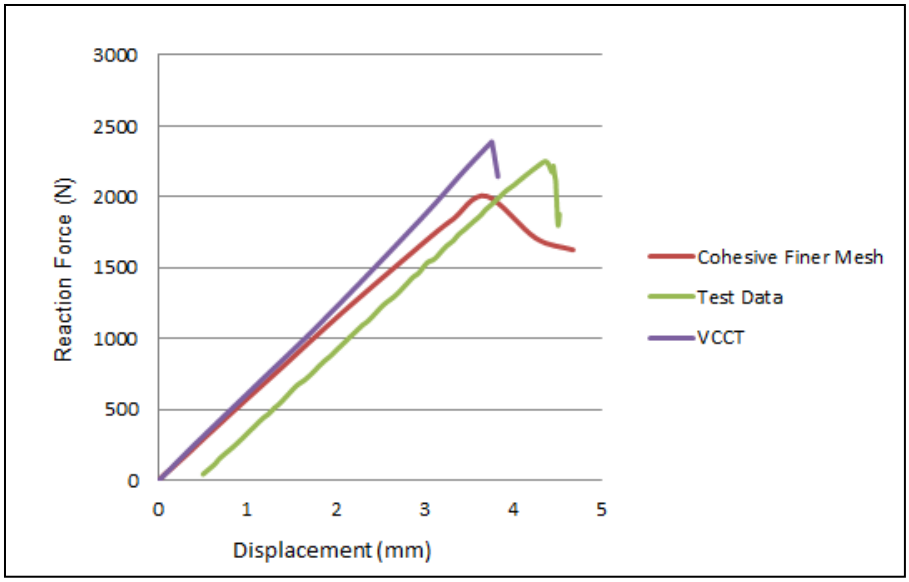

Figure 3-22 Load – Displacement graph for mode II delamination

Thus, as we can see from the results, the graph plotted by ABAQUS, is similar to that provided by CYTEC. The peak loads, that correspond to when the crack starts propagating, and their corresponding crosshead displacements are mentioned in the table below.

Table 3-13 Summary of mode II delamination

MODEL NAME	*PEAK LOAD (N)*	*CROSS HEAD DISP. (mm)*
Test Data by CYTEC Inc.	2249.7	4.3
Analysis with VCCT	2386.4	3.7
Analysis with CZM	2000.6	3.6

CHAPTER 4. MODELING FOUR POINT BEND TEST OF THE I-BEAM

This section documents the damage tolerance analysis performed on a 3-stringer test panel, which is to be tested as part of the TAPAS technology development program. The skin and stringers are made from thermoplastic composite material (Carbon / PEKK) and joined with a butt-joint connection between stringer web and skin.

Fog 4.1 depicts the I-Beam modeled in ABAQUS CAE. The model consists of the two fillers and the web, which are attached by a butt joint. Fig 4.2 is a model of the four point bend test, with two support pins and two loading pins.

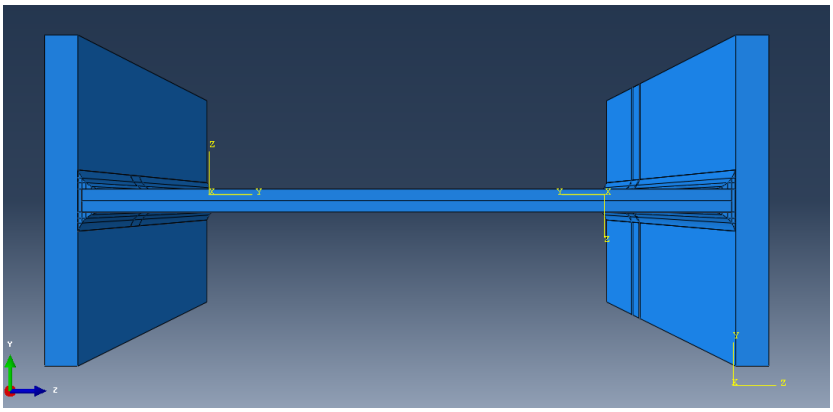

Figure 4-1 I-Beam- Flange, Web and Filler

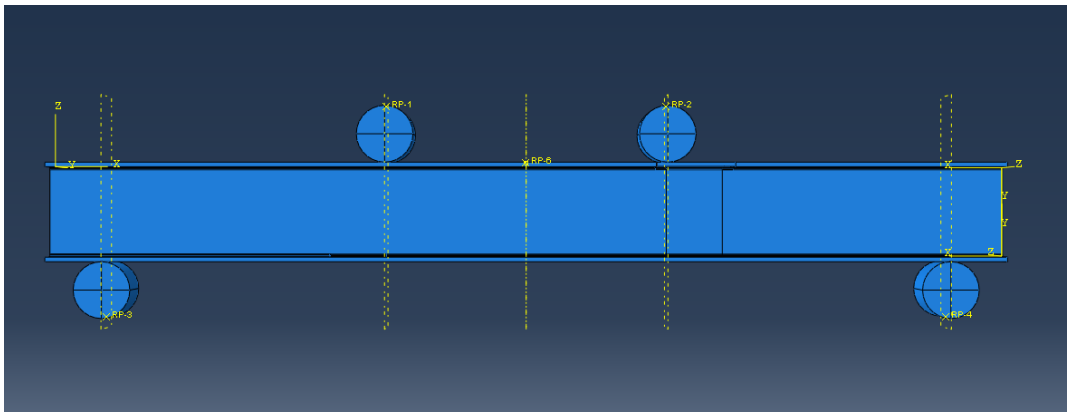

Figure 4-2 The Four-Point bend test apparatus of the I-beam

4.1 Geometry and Idealization

The SI (mm) set of units is used for the FE model, and are shown in Table 4.1

Table 4-1 Consistent units in FE model

Quantity	**SI (mm)**
Length	mm
Force	N
Mass	tonne (10^3 kg)
Time	s
Stress	MPa (N/mm^2)
Energy	mJ (10^{-3} J)
Density	$tonne/mm^3$

The modeling strategy involves subdividing the model into two zones: a “Fine Mesh Zone” in the area of fatigue delamination growth, and a “Coarse Mesh Zone” in the remainder of the panel.

The “Fine Mesh Zone” strategy uses a mesh with regular hexahedral elements to the extent possible. The planform element dimensions are ~1 mm, and the through-thickness mesh is 1 element per ply for the top 3 plies at the delamination interface. Identical surface meshes are imposed at all part interfaces. A detailed view of the “Fine Mesh Zone” is shown in Figure 4.3.

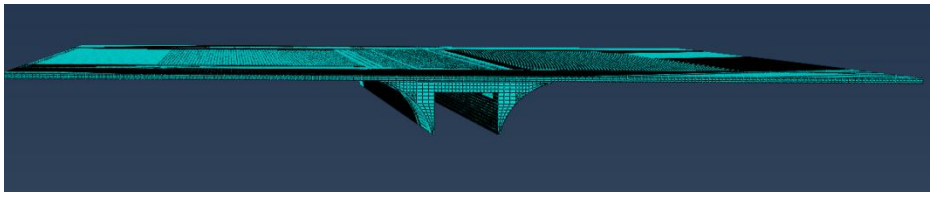

Figure 4-3 Fine Mesh Region of the I-Beam

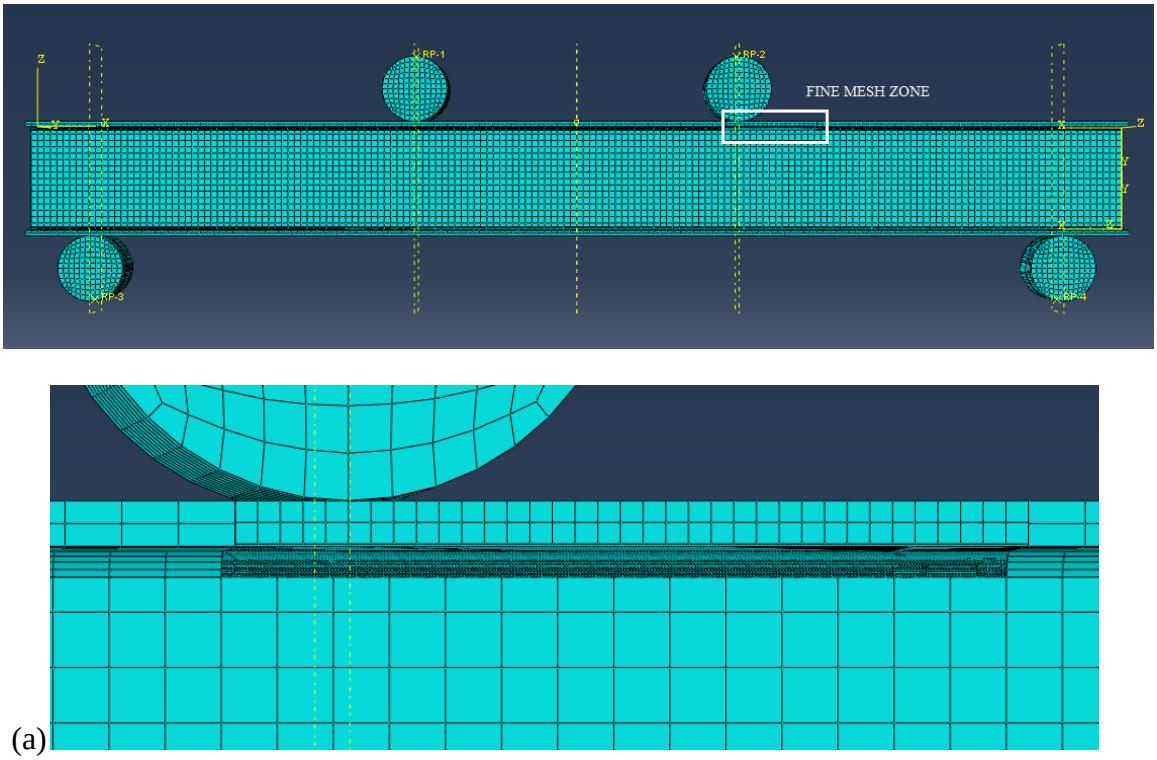

(a)

(b)

Figure 4-4 The fine mesh zone (a) with exploded view (b)

The “Coarse Mesh Zone” strategy uses a relatively coarse mesh (sufficient to capture the panel stiffness and stability response). The planform element dimensions are ~4 – 10 mm and 2 element through the thickness of each structural member. The ABAQUS surface “tying” strategy is used to connect the Coarse Mesh Zone to the Fine Mesh Zone.

4.1.1 Fine Mesh Filler

The fine mesh skin is modeled with 5 elements through the thickness. The top 4 plies (directly above the filler) are each modeled with a single element through the thickness. The remainder of the skin layup is modeled with one element, representing the next 55 plies in the 58 ply layup, see Fig 4.5.

The ply-by-ply refinement (top 3 plies) at the delamination interface allows for discrete material property definition for each ply. In addition, the approach enables the analysis of a delamination between these skin plies in the future.

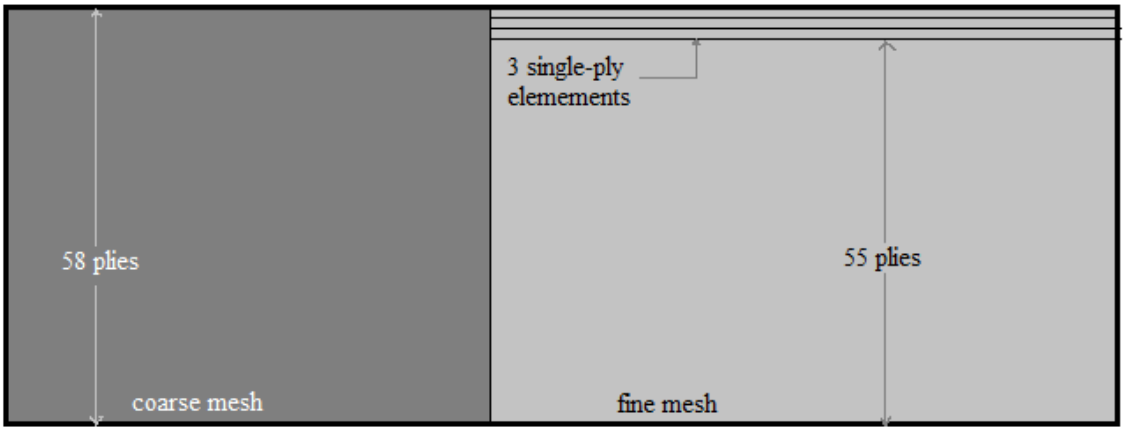

Figure 4-5 Fine Mesh Zone through-thickness skin modeling approach

4.1.2 Fine Mesh Filler

The filler consists of the butt joint between the Flange and the Web, where the pre-crack lies. It is the most complex portion and includes a small number of tying constraints, similar to those used between the coarse and fine mesh zones of the model. Performance of the elements is critical, since the initial delamination under investigation is between the filler and the skin. The tip of the filler geometry is truncated by 1.28 mm on each side, which corresponds to a thickness of 0.138 mm (one ply thickness), to avoid the use of six-noded wedge elements (C3D6), as shown in Fig 4.6.

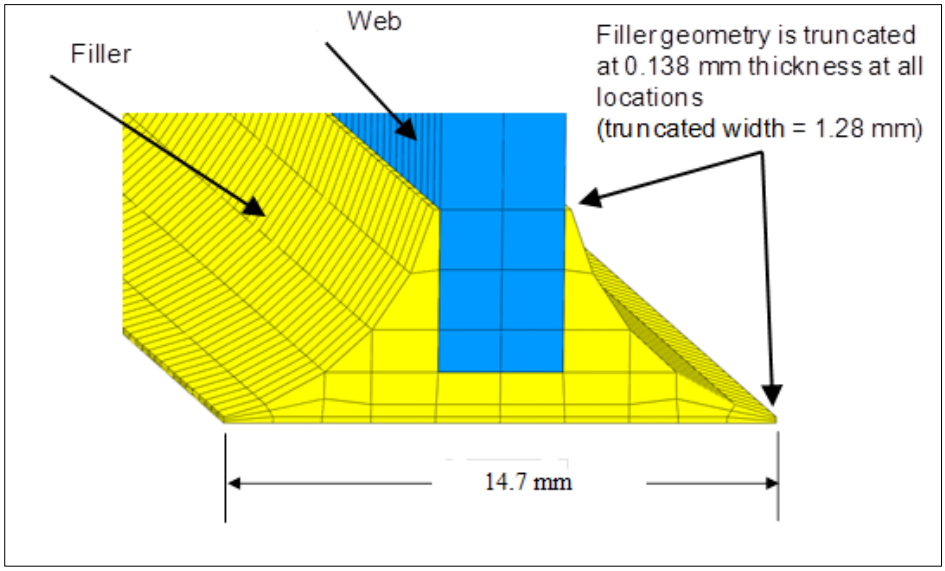

Figure 4-6 Truncated filler geometry

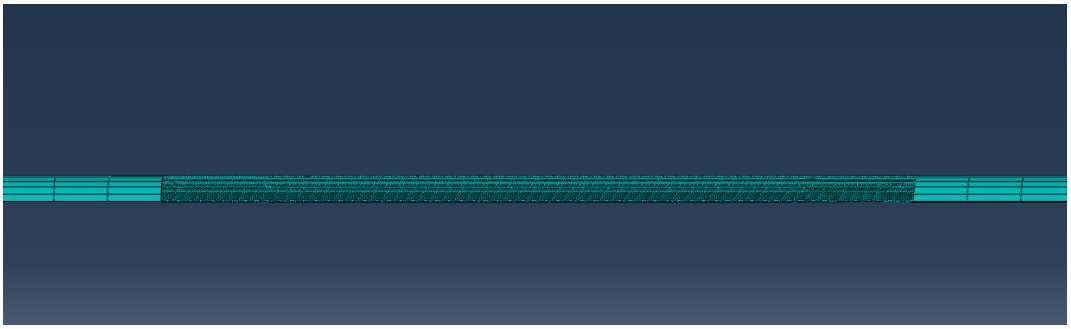

Figure 4-7 Fine mesh zone of the filler length

4.2 Material Properties

The material properties used in the analysis are shown in table 4.2 through table 4.4. Material properties for the ASD4/PEKK material were supplied by Fokker, in coordination memos and email correspondence. Material properties for aluminum were defined as "Typical" industry values.

Table 4-2 3D Ply Properties for ASD4/PEKK

Property	***Value***	***Unit***
E_1	133450	N/mm^2
E_2	10800	N/mm^2
E_3	5460	N/mm^2
ν_1	0.319	
ν_2	0.319	
ν_3	0.02	
G_{12}	5460	N/mm^2
G_{13}	5460	N/mm^2
G_{23}	5088	N/mm^2
Ply Thickness	0.138	mm

Table 4-3 Properties for Filler

Property	***Value***	***Unit***
E	$1.31 * 10^4$	N/mm^2
ν	0.4	

Table 4-4 Properties of Steel (Loading/Support Pins)

Property	***Value***	***Unit***
E	$2 * 10^5$	N/mm^2
ν	0.3	

4.3 Laminate Definitions

Laminate definitions for the coarse mesh region of the FE model use the ABAQUS `*SOLID SECTION, COMPOSITE`, option. This input option uses a ply-by-ply definition of the laminate stack. Laminate definitions for the fine mesh stringer also use the ABAQUS `*SOLID SECTION, COMPOSITE` option. The fine mesh skin region uses individual elements for the first 3 IML plies and 3 elements for the next 55 plies in the 58-ply layup. Properties for the first 3 IML plies are defined in the fiber direction and rotated to the appropriate angle using the `*ORIENTATION` option. Properties for the remainder of the sub-laminate are defined with the `*SOLID SECTION, COMPOSITE` option.

Laminate definitions for the flange and web are given in table 4.5. Note: The 0° fiber direction is aligned with the global axial X direction.

Table 4-5 Layup Definitions for I-Beam

Section	*Source*	*Layup*
Flange – 58 Ply	TW-14-086	-45/0/0/45/90/90/-45/0/-45/0/45/90/45/90/-45/0/45/90/-45/0/45/90/-45/0/45/90/-45/0/45/90/-45/45/0/90/45/-45/90/45/0/-45/90/45/0/-45/90/45/0/-45/90/45/90/45/0/-45/0/-45/90/90/45/0/0/0
Web – 40 Ply	TW-14-086	$[-45/90/45/0/-45/90/45/0/-45/90/45/0/-45/90/45/0/-45/90/45/0]_s$

4.4 Boundary Conditions and Constraints

Like in mode II delamination, the four pins ae modeled as rigid bodies, whose motion is controlled by their corresponding reference points.

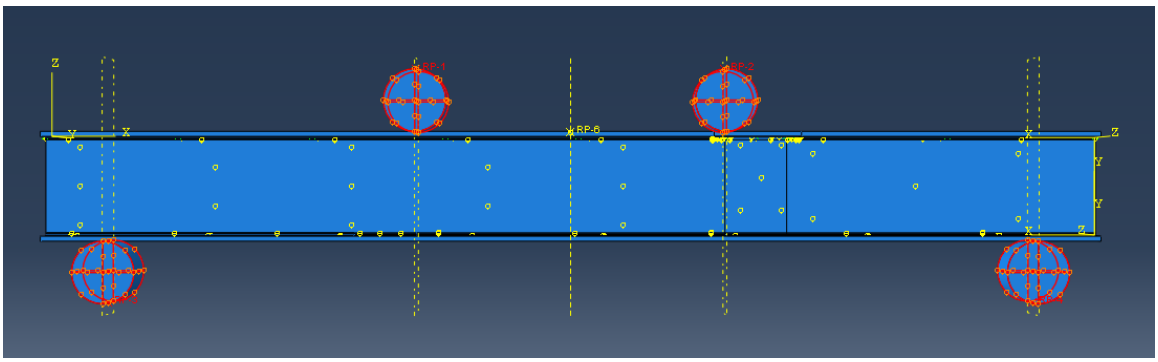

Figure 4-8 Support Pins modeled as rigid bodies

These loading pins are grounded or given a displacement loading as in Mode II. However, an additional boundary condition is added to this experiment. A node set is defined comprising of the nodes on the middle perimeter of the I-Beam (as shown in

figure). These nodes are given an additional boundary condition. They are allowed motion only along X and Y direction. Their degree of freedom along z direction is restricted to avoid the I-Beam from any unwanted motion.

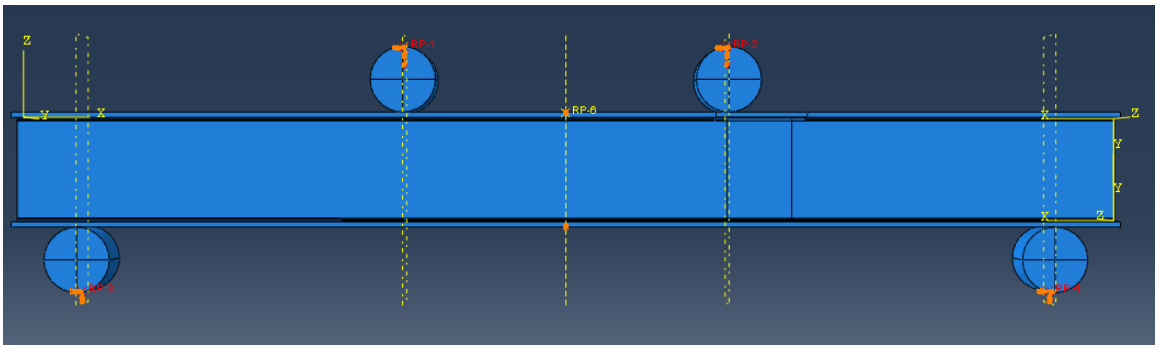

Figure 4-9 Boundary conditions on the support pins

Table 4-6 Boundary Conditions on the support pins

Node Set	**U_1**	**U_2**	**U_3**
Loading Pins (RP1, RP2)	0	0	-15 mm
Support Pins (RP2, RP3)	0	0	0
Mid Nodes	-	-	0

4.5 Interactions

There are two sets of interactions acting on this model. The first comprises of interactions acting between the roller pins and the I-Beam. They have a normal and tangential interaction like described in mode II.

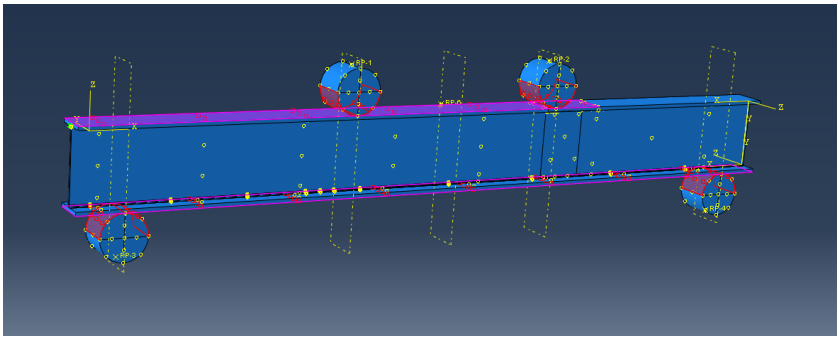

Figure 4-10 Interactions between support pins and I-Beam

The next set of interaction if applying the VCCT and CZM. The delamination acts between the top filler and the flange, as show in the figure below. The interaction properties are the same as used in Mode II and Mode I.

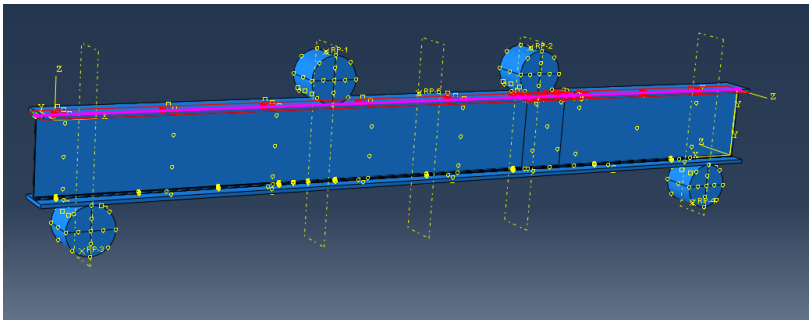

Figure 4-11 Interactions between top flange and filler

The delamination is again mentioned by the bonded and un-bonded node set. The bonded set is shown below. The initial delamination used is 100 mm. The selected node set below shows the bonded region in the model set up.

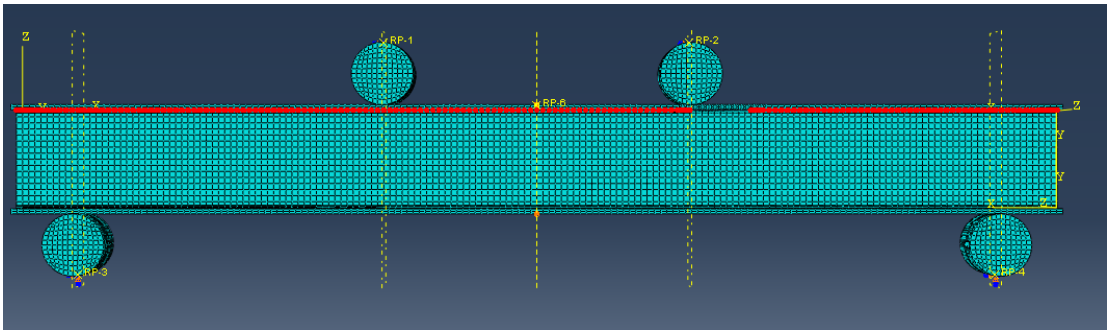

Figure 4-12 Bonded region of the I-Beam

We get a better understanding when we look at the finely meshed zone, specifically the finely meshed filler which contains the bonded nodes. The highlighted nodes represent the area which is bonded initially. The unbounded area is the pre crack which corresponds to 100 mm.

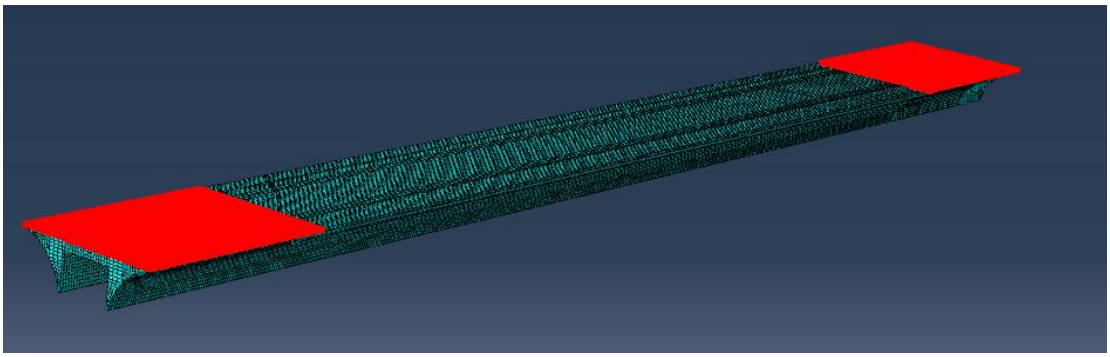

Figure 4-13 Bonded region in the Fine Mesh Zone: Filler

4.6 Results

4.6.1 VCCT Model

On application of displacement loading on the loading pins, the I-Beam bends undergoing mode II delamination at the crack fronts. The analysis is made to run till the maximum displacement was -8.1 mm in z direction (due to time constraints). The corresponding stresses for this displacement are shown in the figure below.

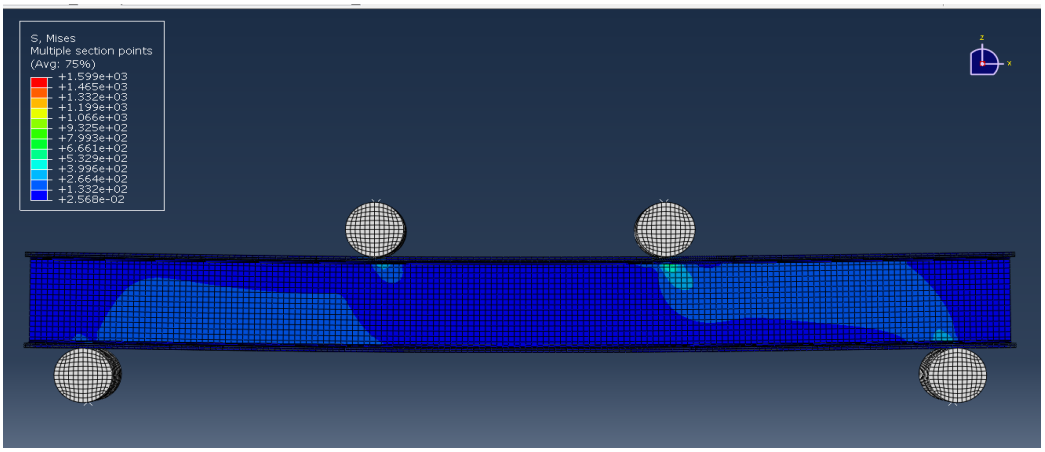

Figure 4-14 Stresses acting on deformed body: VCCT

We can observe a slight asymmetry on the stress distribution due to the existence of a crack on the right hand side of the I-Beam. The first thing to observe would be the reaction force v/s displacement graph for the loading pins, and look for differences. But on plotting the two graphs from the results obtained in ABAQUS, we observe no dissimilarities between the loading pins. Hence, no information about the delamination can be obtained from this method.

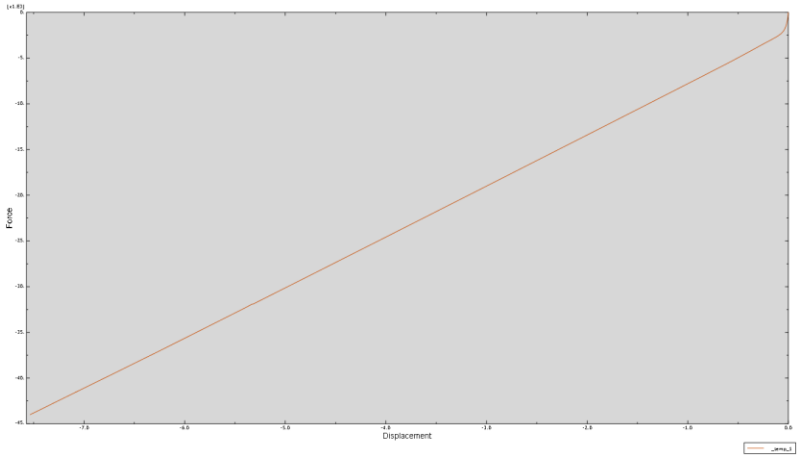

(a)

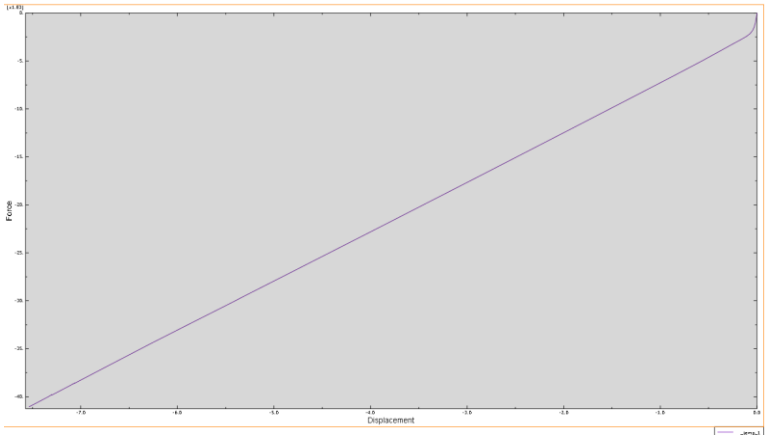

(b)

Figure 4-15 Reaction force v/s Displacement for (a) Loading pin 1 (b) Loading Pin 2

The next parameter to analyze is the finely meshed zone of the model. The parameter used to study the delamination using VCCT in ABAQUS is the EFENRRTR. This corresponds to ratio between the energy release rate per element to its critical energy release rate, as mentioned during interactions. Once the ratio exceeds 1, we know the element is not bonded and the crack is propagating.

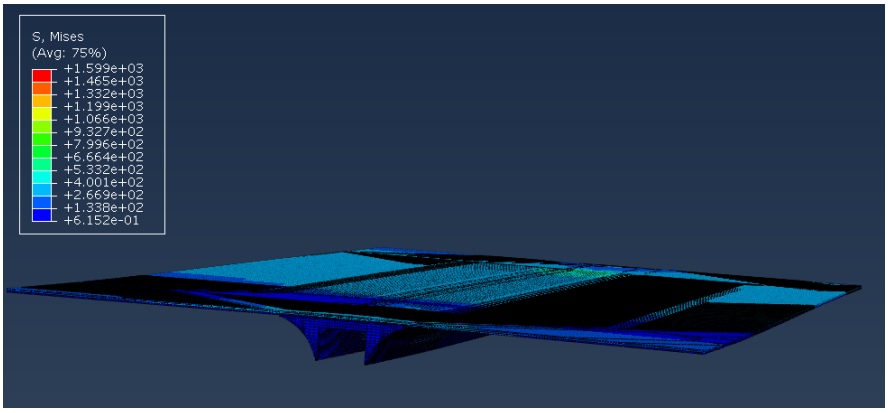

Figure 4-16 Stress distribution in fine mesh zone: VCCT

Thus, the EFENRRTR is observed for the fine mesh filler, which consist of the nodes that are initially bonded. The figure below shows the EFENRRTR for every element on the filler.

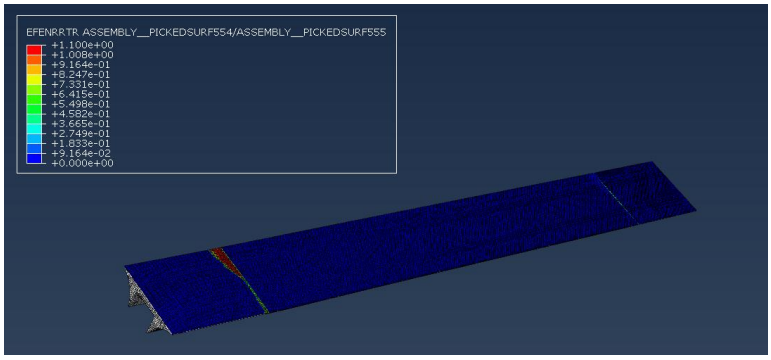

Figure 4-17 The EFENRRTR distribution over the filler

From the figure we can observe that the region highlighted in red represent the elements which have debonded. Thus, a more appropriate graph to plot is the EFENRRTR v/s vertical displacement for selected nodes.

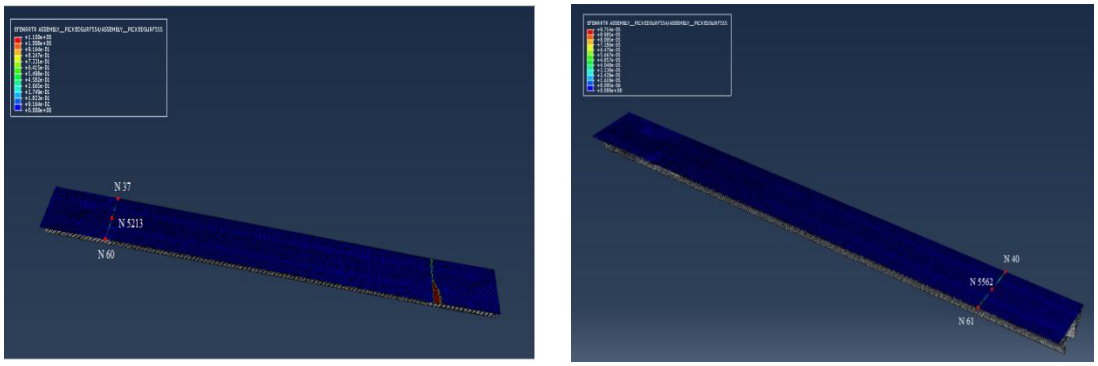

Figure 4-18 Six nodes on the crack front

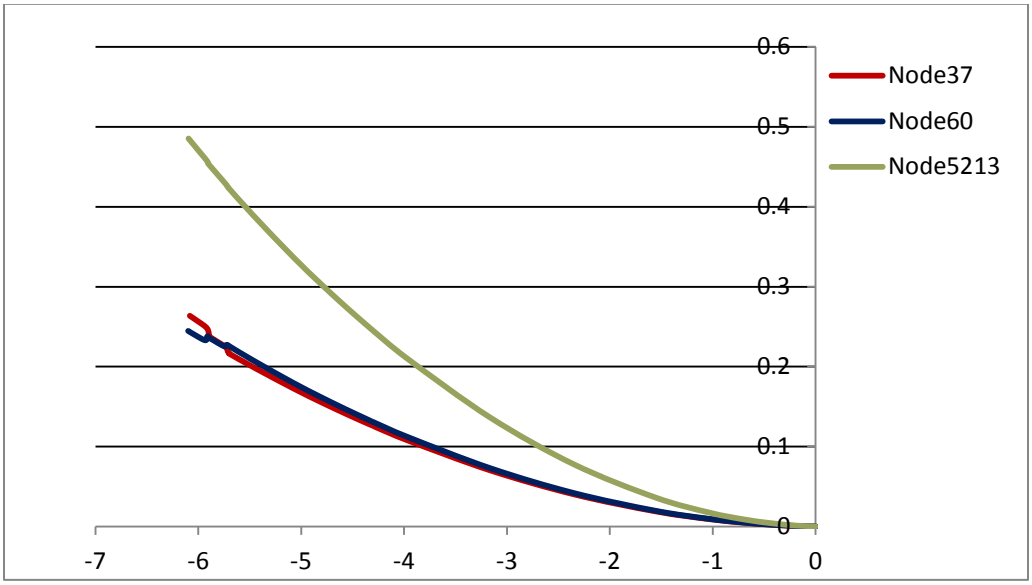

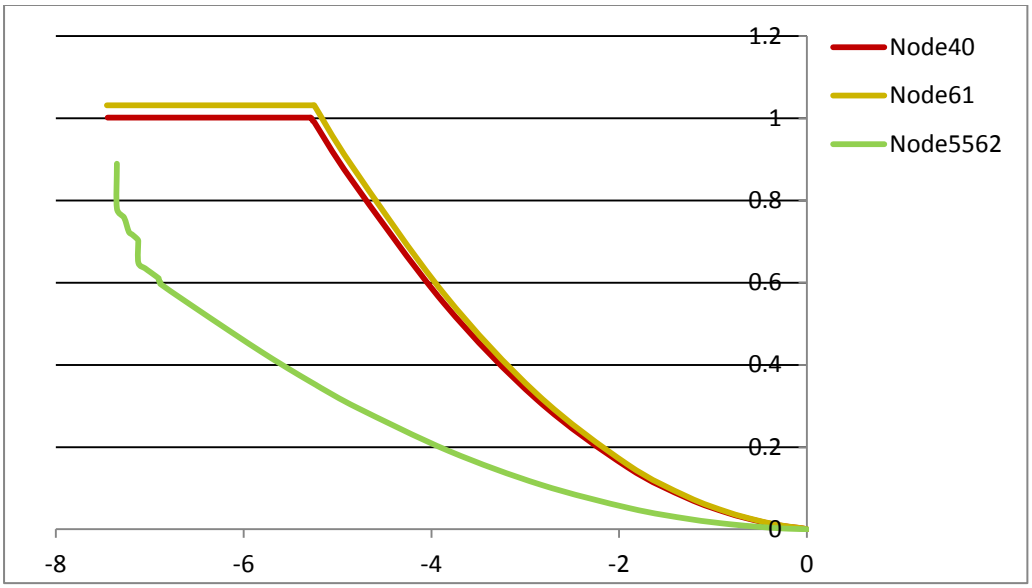

Figure 4-19 EFENNRTR v/s displacement for the six selected nodes

Thus, we can see from the figure that Node 61 is the first to debond. Node 61 lies on the crack-front that lies directly below the loading pin 2. Corresponding to the Reactions force v/s displacement graph for that pin, we can identify the load at which the crack starts propagating for the I-Beam.

Table 4-7 Summary of VCCT model

Node	Node Disp. (mm)	Corresponding LP2 disp. (mm)	Reaction Force at LP2 (N)
61	-5.248	-5.315	-29550.9

4.6.2 CZM Model

Similar to the previous section, the delamination in the cohesive can be studies through a parameter named ‘CSDMG’, which is also a ratio of the maximum energy released to the critical energy release. Every time the parameter reaches 1, implies the

bonded region has started delaminating. Again, 6 node points were chosen along the crack fronts and their CSDMG was plotted as a function of vertical displacement.

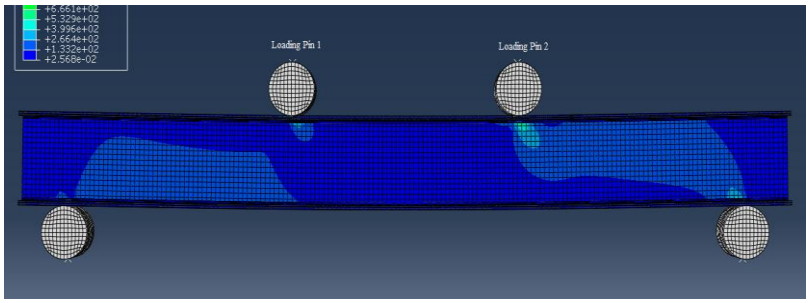

Figure 4-20 Stresses acting on final deformed model: CZM

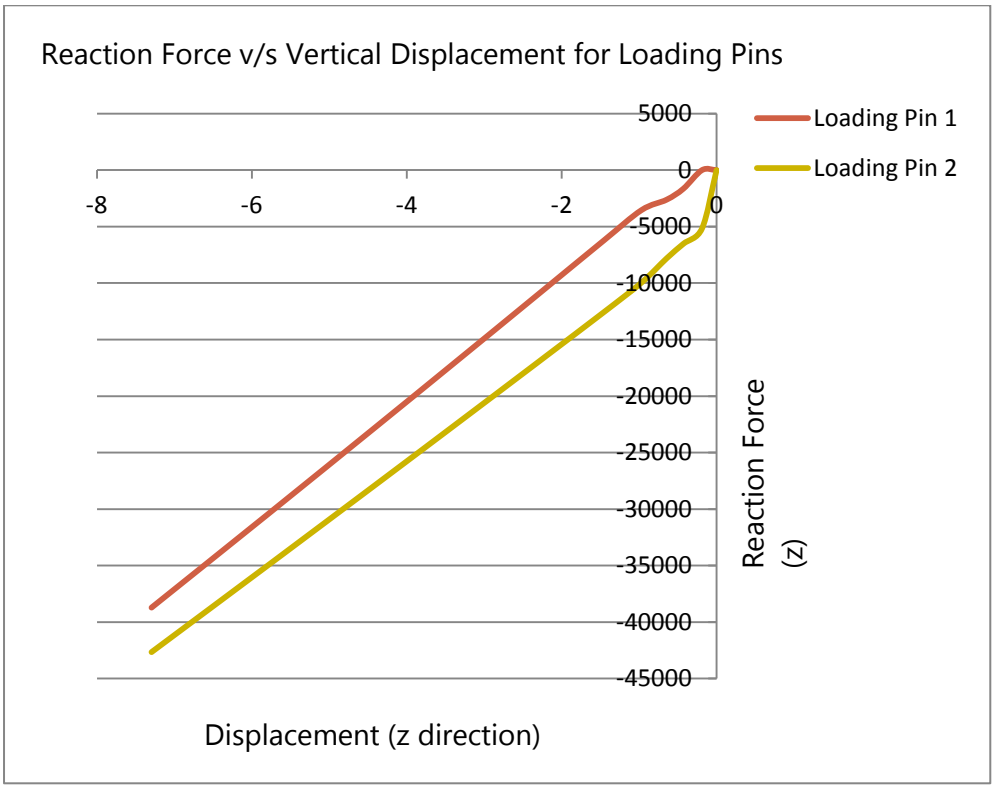

Figure 4-21 Reaction Force v/s Displacement for Loading Pins: CZM

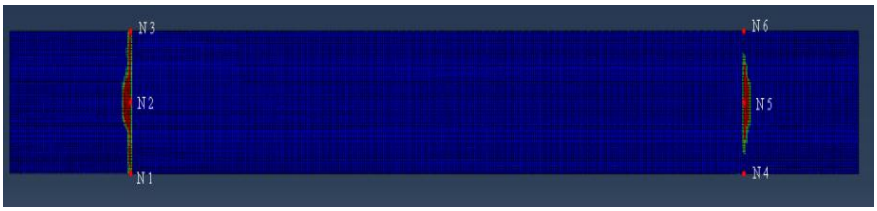

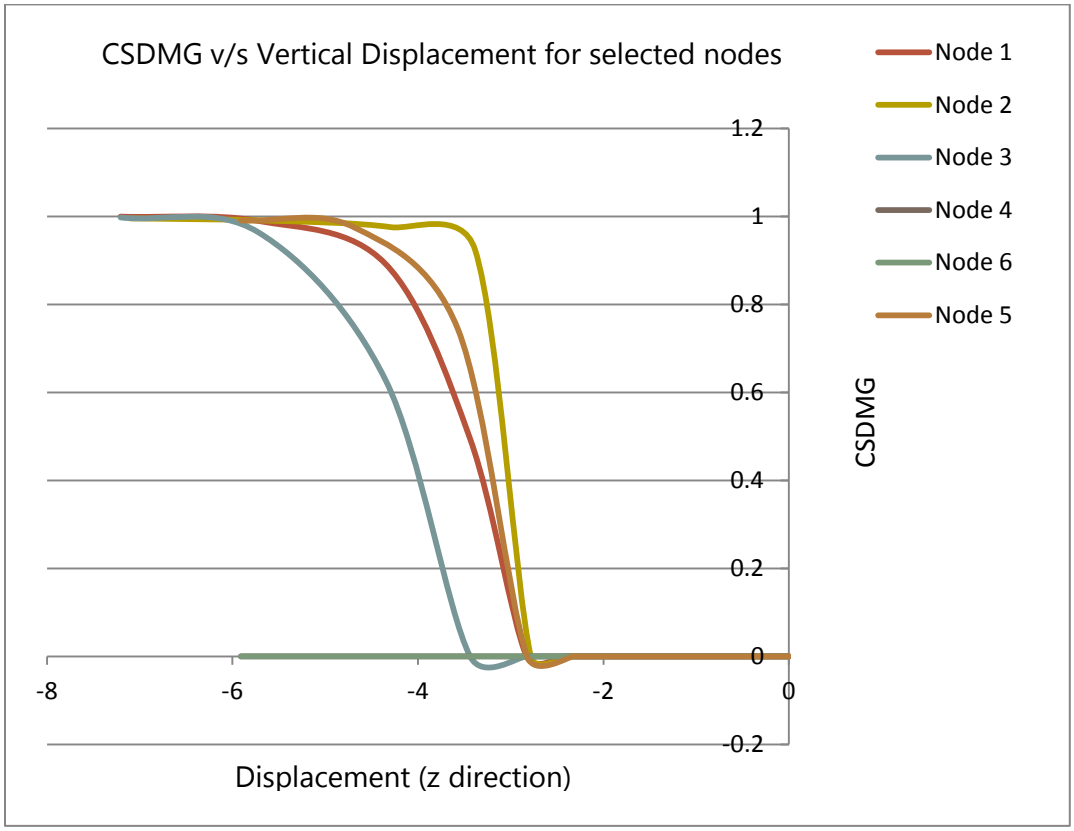

Figure 4-22 CSDMG v/s Vertical Displacement for selected nodes: CZM

However, an interesting observation made while plotting the reaction forces – displacement graph for the two loading pins are not identical like they were in the previous model. The crack front below the Loading pin 2 does however start to propagate first, but the middle node starts delaminating first.

Table 4-8 Summary of Cohesive Zone Model

Node	Node Disp. (mm)	Corresponding LP2 disp. (mm)	Reaction Force at LP2 (N)
2	-5.564	-5.795	-34993.9

4.7 Observations

Both the models, using virtual crack closure technique and cohesive damage mechanics, give similar results. Both models predict crack growth when the vertical displacement of the loading pins is about 5.5 mm (average) in the negative z direction, which corresponds to approximately 31kN (average) force in the negative z direction.

Table 4-9 Summary for I-Beam

Method	Corresponding LP2 disp. (mm)	Reaction Force at LP2 (N)
VCCT	-5.315	-29550.9
CZM	-5.795	-34993.9
Avg.	-5.555	-32272.4

From the data provided by Fokker Aerostructures, the loads acting on web of Section N of the center beam corresponded to 273 N/mm. The distance between the loading pin and the support pin is 500 mm. This translates to a point load of 136,500 N on the loading pin. Thus, we can safely say the crack will propagate within the range of loads applied.

However, there are two distinct differences between the VCCT and the CZM models. The first is the reaction force-displacement graphs of the two loading pins. According to the VCCT models, they are exactly alike, but the CZM models display a variation between the two.

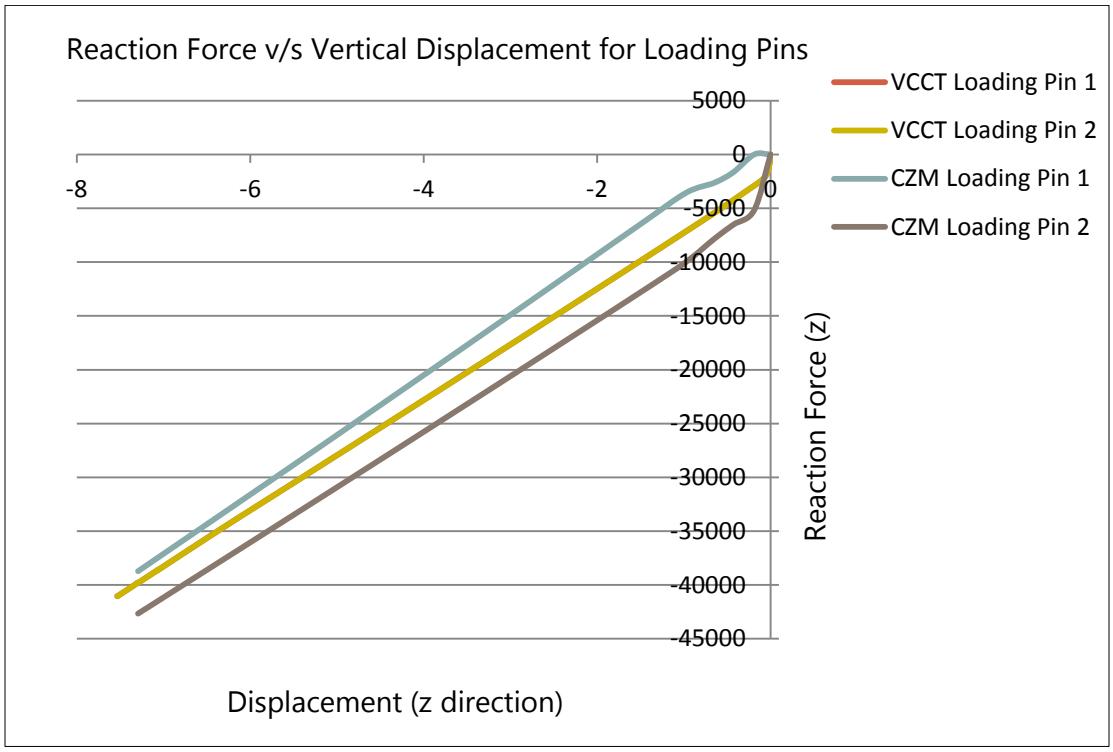

Figure 4-23 Reaction force – displacement curves for CZM and VCCT model

As we can see in the table, for the CZM models, for the same vertical displacement, the reaction forces developed in the Loading pin 2 is much greater than in Loading Pin 1. The virtual crack closure technique however, shows the exact same reaction force for both the loading pins.

Another difference is the location of the crack growth. While Virtual Crack Closure Technique predicts it to be the nodes at the edge of the filler, Cohesive Zone Model predicts it to be at the mid points of the filler.

CHAPTER 5. CONCLUSION

Today, vast majority of composite materials for aerospace are based on thermoset materials. However, the second half of the 1980s saw the emergence of a new family of composite materials, continuous fiber reinforced thermoplastics and for the past few years, they have significantly matured. Their characteristic offers intriguing possibilities for both faster and more innovative composite processing techniques compared to their thermoset counterparts. This lead to the start of the Thermoplastic Primary Aircraft Structure innovation program (TAPAS), a consortium that consists of companies and knowledge institutes in the Dutch aerospace industry working together with the aircraft manufacturer Airbus, which aims to increase the proportion of thermoplastic composites in commercial aircrafts.

For this thesis, the center beam of the Gulfstream 650 aircraft's horizontal tail plane, previously a carbon fiber/epoxy hat-stiffened skin construction is being redesigned using unidirectional carbon fiber/PEKK (Poly-ether-ketone-ketone) composite. An I-Beam is modeled with the dimensions of a certain section of the center beam, along with the loads acting on the carbon epoxy counterpart. However, a pre-crack of 100 mm in inserted in the beam between the top flange and the filler, and a damage analysis is performed to see if the model delaminates within the load range that acts on the current carbon fiber/epoxy model.

To perform the damage analysis on the I-Beam two finite element methods were identified, namely Virtual Crack Closure Technique and Cohesive Zone Model. However, before analyzing the C/PEKK I-Beam, the two methods were first verified by reproducing the experimental data done by Cytec Inc. for determining the fracture toughness (G_{1c} and G_{2c}) in pure mode I and mode II delamination. The experiments followed the standard procedures prescribed by ASTM 5528 for mode I and EN 6034 for mode II bending. To simulate the loading applied on the G650 center beam, the I-Beam was placed under a four point bend, with a constant displacement loading. The model was then analyzed to study the forces at which the crack starts growing, using both VCCT and CZM.

We observe from the results that both finite element approaches produce similar results, which state that the crack starts to grow when the vertical displacement of the load pins are about 5.55 mm and have a reaction force corresponding to 32.27 kN. Thus, considering the loads acting on the carbon fiber/epoxy center beam lie in the magnitude of 136.5 kN, the thermoplastic model will definitely see crack propagation if it has an initial delamination.

Thus, to prevent this there are only two parameters that can be tampered with: the material used and the area of contact between the filler and the flange. The latter parameter can be increased and the filler can be made wider, to increase the contact with the flange. However, the most significant conclusion made from the report is the difference in the modeling cohesive interactions and virtual crack closure technique

in ABAQUS. It was observed that the analysis time required for CZM was significantly lesser than the models using VCCT interactions. With each model analyzed in this project, its complexity progressively increased. First, there was a simple beam with opening loads, next a beam under a three point bend and finally an I-Beam in four-point bend loading condition. With each analysis, the CZM model took one, three and five hour lesser time to complete the job. Thus, we can infer that for more complex models, the cohesive approach is much faster and can save hours of computational time.

Further study can be done on the I-Beam by varying the location and the length of the initial delamination. A through hole can also be modelled to mirror the carbon epoxy center beam and the stresses in the I-Beam can be observed.

REFERENCES

REFERENCES

[1] A. R. Offringa, “Thermoplastic composites—rapid processing applications,” *Compos. Part A Appl. Sci. Manuf.*, vol. 27, no. 4, pp. 329–336, Jan. 1996.

[2] H. Ning, U. Vaidya, G. M. Janowski, and G. Husman, “Design, manufacture and analysis of a thermoplastic composite frame structure for mass transit,” *Compos. Struct.*, vol. 80, no. 1, pp. 105–116, Sep. 2007.

[3] M. Hou, L. Ye, H. J. Lee, and Y. W. Mai, “Manufacture of a carbon-fabric-reinforced polyetherimide (CF/PEI) composite material,” *Compos. Sci. Technol.*, vol. 58, no. 2, pp. 181–190, Jan. 1998.

[4] J. Denault and M. Dumouchel, “Consolidation process of PEEK/carbon composite for aerospace applications,” *Adv. Perform. Mater.*, 1998.

[5] I. Chang, “PEKK as a new thermoplastic matrix for high-performance composites,” *SAMPE Q.;(United States)*, 1988.

[6] A. Goldberg, “Screening of matrices and fibers for reinforced thermoplastics intended for dental applications,” *J. Biomed. ...*, 1994.

[7] E. Wang and T. Gutowski, “Cost comparison between thermoplastic and thermoset composites,” *SAMPE J.*, 1990.

[8] A. Offringa, “Structural Thermoplastic Aircraft Floor Panels--in Series Production,” *Soc. Adv. Mater. Process ...*, 1994.

[9] G. Marsh, “Reinforced thermoplastics, the next wave?,” *Reinf. Plast.*, 2014.

[10] P. F. Liu, S. J. Hou, J. K. Chu, X. Y. Hu, C. L. Zhou, Y. L. Liu, J. Y. Zheng, A. Zhao, and L. Yan, “Finite element analysis of postbuckling and delamination of composite laminates using virtual crack closure technique,” *Compos. Struct.*, vol. 93, no. 6, pp. 1549–1560, May 2011.

[11] D. Sleight, “Progressive failure analysis methodology for laminated composite structures,” 1999.

[12] M. R. Garnich and V. M. K. Akula, “Review of Degradation Models for Progressive Failure Analysis of Fiber Reinforced Polymer Composites,” *Appl. Mech. Rev.*, vol. 62, no. 1, p. 010801, 2009.

[13] P. F. Liu and J. Y. Zheng, “Recent developments on damage modeling and finite element analysis for composite laminates: A review,” *Mater. Des.*, vol. 31, no. 8, pp. 3825–3834, Sep. 2010.

[14] V. Ranatunga, “Finite element modeling of delamination crack propagation in laminated composites,” *Proc. World Congr. Eng. …*, 2011.

[15] E. Rybicki and M. Kanninen, “A finite element calculation of stress intensity factors by a modified crack closure integral,” *Eng. Fract. Mech.*, 1977.

[16] I. Raju, “Calculation of strain-energy release rates with higher order and singular finite elements,” *Eng. Fract. Mech.*, 1987.

[17] G. . Barenblatt, “The formation of equilibrium cracks during brittle fracture. General ideas and hypotheses. Axially-symmetric cracks,” *J. Appl. Math. Mech.*, vol. 23, no. 3, pp. 622–636, Jan. 1959.

[18] D. S. Dugdale, “Yielding of steel sheets containing slits,” *J. Mech. Phys. Solids*, vol. 8, no. 2, pp. 100–104, May 1960.

[19] H. Hibbitt, B. Karlsson, and P. Sorensen, “Abaqus Analysis User’s Manual Version 6.10,” *Dassault Systèmes Simulia Corp. Provid. RI, …*, 2011.

[20] M. Kachanov, “Effective elastic properties of cracked solids: critical review of some basic concepts,” *Appl. Mech. Rev.*, 1992.

[21] M. Kachanov, “Elastic solids with many cracks and related problems,” 1993.

[22] H. Chai, C. D. Babcock, and W. G. Knauss, “One dimensional modelling of failure in laminated plates by delamination buckling,” *Int. J. Solids Struct.*, vol. 17, no. 11, pp. 1069–1083, Jan. 1981.

[23] G. Kardomateas, A. Pelegri, and B. Malik, “Growth of internal delaminations under cyclic compression in composite plates,” *… Mech. Phys. …*, 1995.

[24] G. Kardomateas and D. Schmueser, “Buckling and postbuckling of delaminated composites under compressive loads including transverse shear effects,” *AIAA J.*, 1988.

[25] A. J. Kinloch, Y. Wang, J. G. Williams, and P. Yayla, “The mixed-mode delamination of fibre composite materials,” *Compos. Sci. Technol.*, vol. 47, no. 3, pp. 225–237, Jan. 1993.

[26] J. Reeder, “3D mixed-mode delamination fracture criteria–an experimentalist’s perspective,” 2006.

[27] J. R. Willis, “A comparison of the fracture criteria of griffith and barenblatt,” *J. Mech. Phys. Solids*, vol. 15, no. 3, pp. 151–162, May 1967.

[28] A. Hillerborg, M. Modéer, and P.-E. Petersson, “Analysis of crack formation and crack growth in concrete by means of fracture mechanics and finite elements,” *Cem. Concr. Res.*, vol. 6, no. 6, pp. 773–781, Nov. 1976.

[29] B. Davidson and W. Zhao, “An accurate mixed-mode delamination failure criterion for laminated fibrous composites requiring limited experimental input,” *J. Compos. Mater.*, 2007